Supporting Information

Novel π-extended hybrid xanthene dyes with two spirolactone rings for optoelectronic and biological applications

Qing Wang,[a,b] Xiaojie Jiao,[b] Chang Liu,[b] Kun Huang,[c] Song He,[b] Liancheng Zhao[a,b] and Xianshun Zeng*,[a,b]

[a] *School of Materials Science and Engineering, Harbin Institute of Technology, Harbin 150001, China.*

[b] *Tianjin Key Laboratory for Photoelectric Materials and Devices, School of Materials Science & Engineering, Tianjin University of Technology, Tianjin 300384, China. Email: xshzeng@tjut.edu.cn.*

[c] *School of Chemistry and Chemical Engineering, China West Normal University, Nanchong 637002, China*

Table of Contents

Table S1. Crystal data for *cis*-**S1**.

Item analys	Data
Empirical formula	$C_{42}H_{29}NO_7$
Formula weight	659.66
Temperature/K	299.68(10)
Crystal system	monoclinic
Space group	P2/n
a/Å	12.6280(4)
b/Å	12.0003(3)
c/Å	26.2562(8)
α/°	90
β/°	96.197(3)
γ/°	90
Volume/Å^3	3955.6(2)
Z	4
ρ_{calc}g/cm^3	1.108
μ/mm^{-1}	0.616
F(000)	1376.0
Crystal size/mm^3	0.35 × 0.2 × 0.15
Radiation	CuKα (λ = 1.54184)
2Θ range for data collection/	7.366 to 147.846
Index ranges	$-13 \leq h \leq 15$, $-11 \leq k \leq 14$, $-32 \leq l \leq 32$
Reflections collected	21933
Independent reflections	7557 [R_{int} = 0.0652, R_{sigma} = 0.0596]
Data/restraints/parameters	7557/42/459
Goodness-of-fit on F^2	1.052
Final R indexes [I>=2σ (I)]	R_1 = 0.0974, wR_2 = 0.2989
Final R indexes [all data]	R_1 = 0.1121, wR_2 = 0.3150

Table S2. The stepwise association constants (K_{d1} and K_{d2}) of the *cis*- and *trans*-stereoisomers of **S1** and **S2** with Hg^{2+} ions

Dyes	K_{d1}	K_{d2}
cis-**S1**	8.07 μM	30.85 μM
trans-**S1**	7.2 μM	485 μM
cis-**S2**	9.5 μM	429.5 μM
trans-**S2**	7.45 μM	615 μM

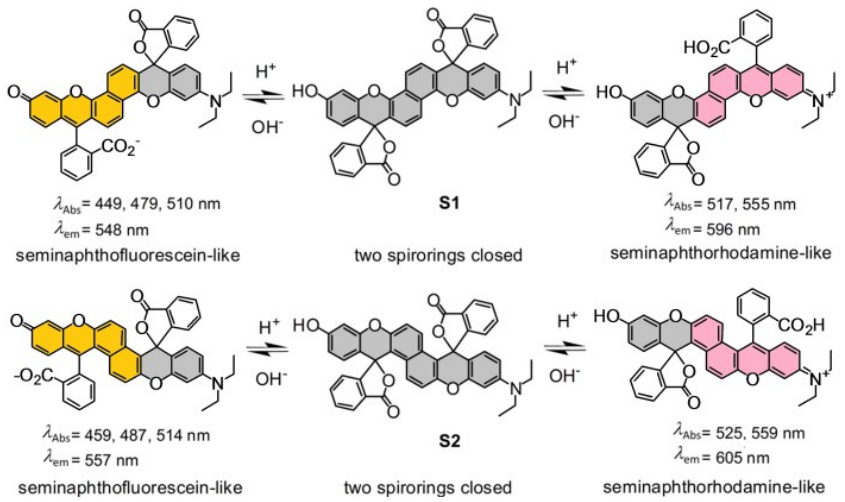

Scheme S1 Proposed spirolactone ring-opening processes of dyes **S1** and **S2** upon additions of OH^- and H^+ in methanol.

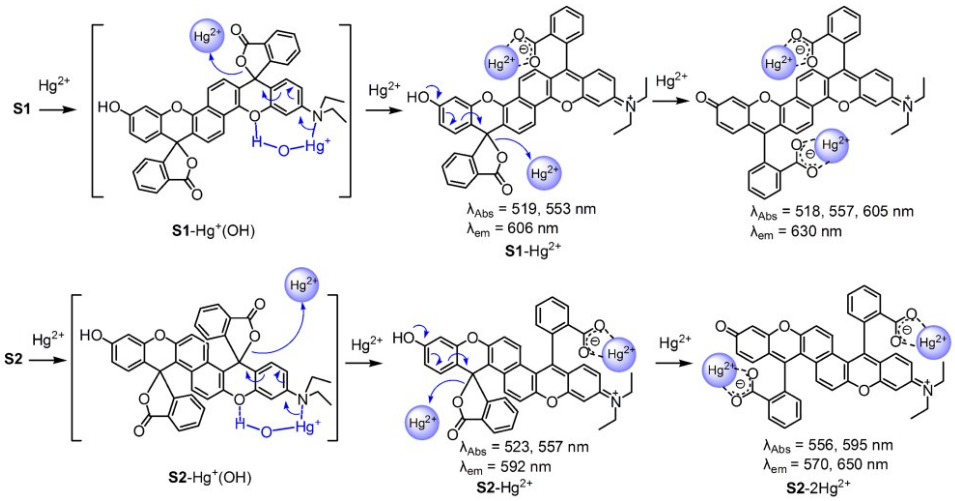

Scheme S2 Proposed spirolactone ring-opening processes of dyes **S1** and **S2** elicited by Hg^{2+} in methanol.

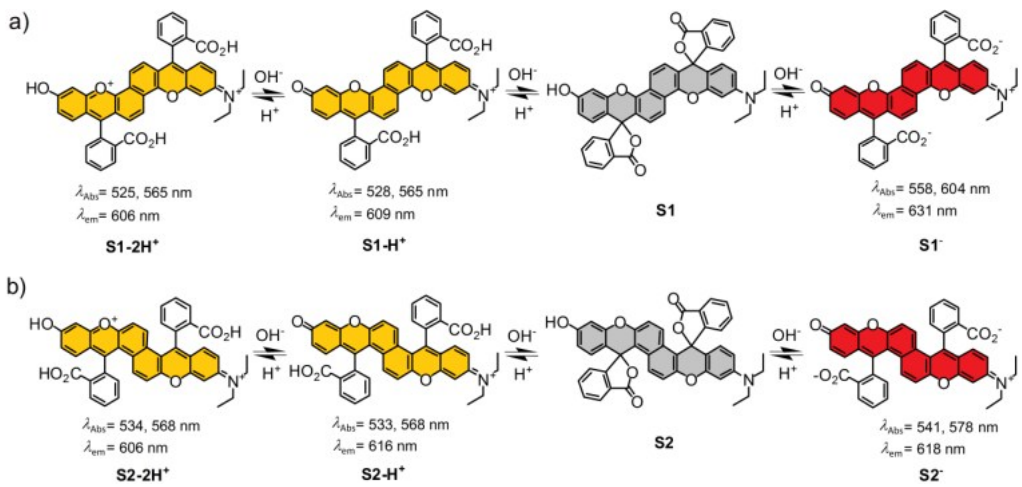

Scheme S3 Proposed pH-dependent equilibrium of dyes **S1** and **S2** in H_2O.

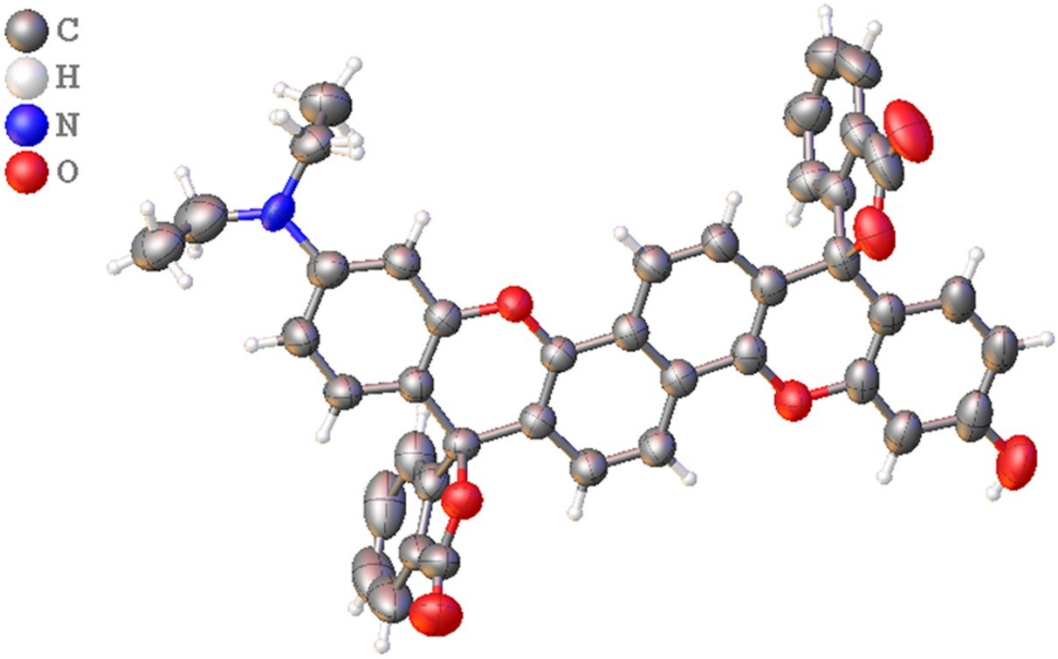

Fig. S1. Crystal structure of *cis*-**S1** with ellipsoid shown at the 50% probability level. *

* The single crystal of *cis*-**S1** for X-ray crystallographic studies was obtained by recrystalization of *cis*-**S1** from DMSO. The crystal Data were obtained by Rigaku SCX-mini diffractometer at 299.68(10) K. The structure was solved by direct method using the SHELXS program of the SHELXTL package and refined by full-matrix least-squares methods with SHELXL. The disordered ethyl group was processed with SHELXL and the solvents of disordered DMSO and water molecules were subtracted using SQUEEZE facility of PLATON.

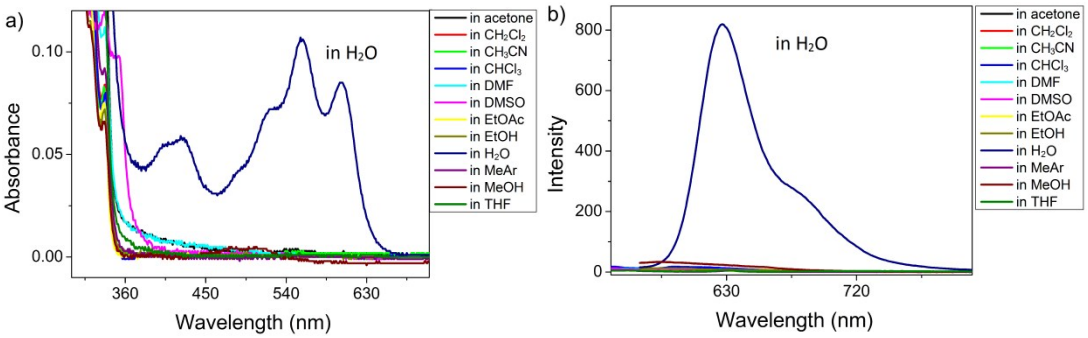

Fig. S2. a) UV/vis absorption and b) fluorescence emission spectra of the dye **S1** in different solvents.

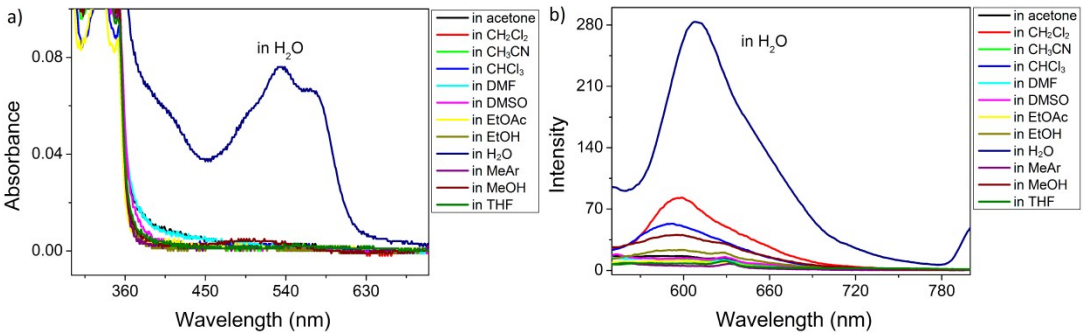

Fig. S3. a) UV/vis absorption and b) fluorescence emission spectra of the dye **S2** in different solvents.

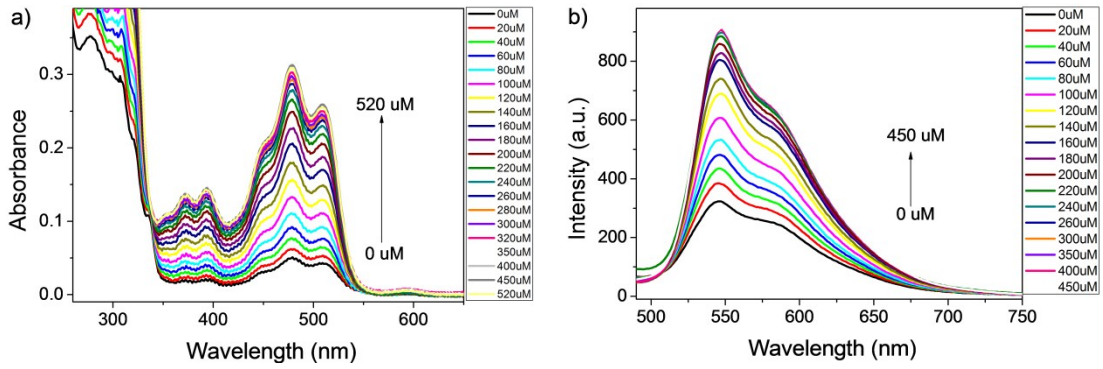

Fig. S4. a) UV-Vis absorption (20 μM) and b) fluorescence spectra (5 μM) of dye *trans*-**S1** after the additions of OH^- in methanol, λ_{ex} = 470 nm; slit: 10 nm, 10 nm.

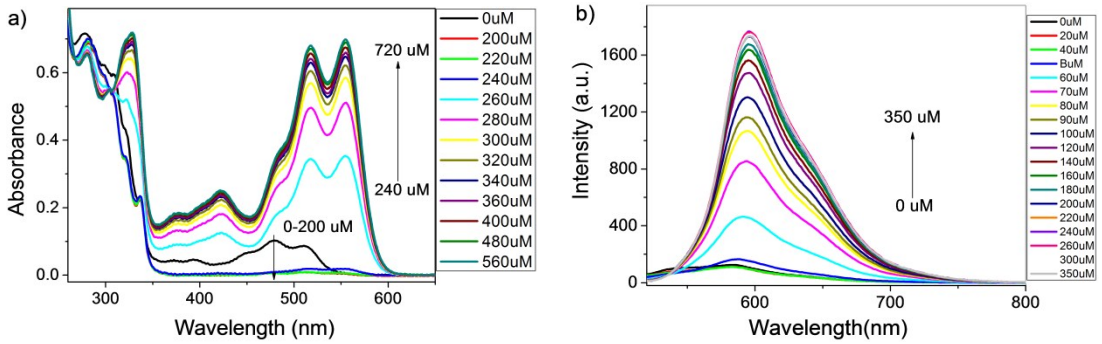

Fig. S5. a) UV-Vis absorption (20 μM) and b) fluorescence spectra (5 μM) of dye *trans*-**S1** after the additions of H^+ in methanol, λ_{ex} = 500 nm; slit: 10 nm, 10 nm.

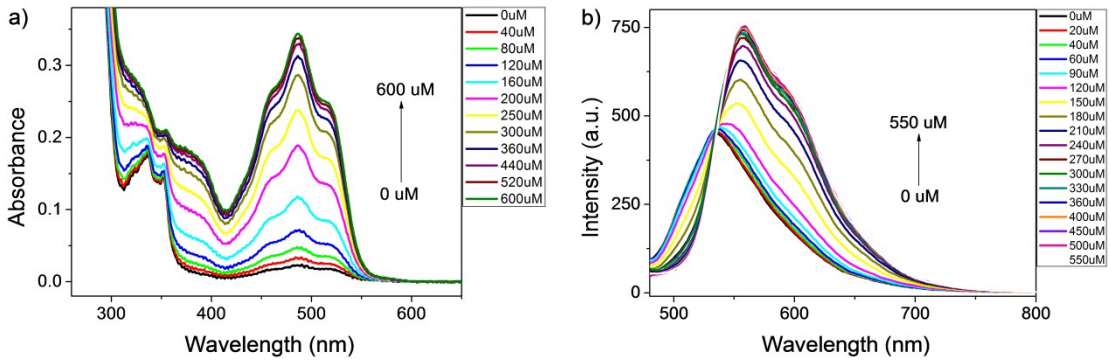

Fig. S6. a) UV-Vis absorption (20 μM) and b) fluorescence spectra (5 μM) of dye *trans*-**S2** after the additions of OH^- in methanol, λ_{ex} = 460 nm; slit: 10 nm, 10 nm.

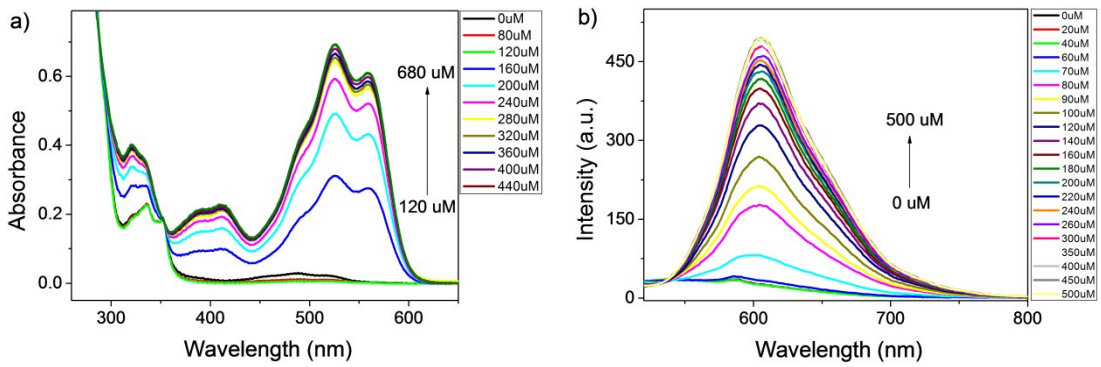

Fig. S7. a) UV-Vis absorption (20 μM) and b) fluorescence spectra (5 μM) of dye *trans*-**S2** after the additions of H^+ in methanol, λ_{ex} = 500 nm; slit: 5 nm, 10 nm.

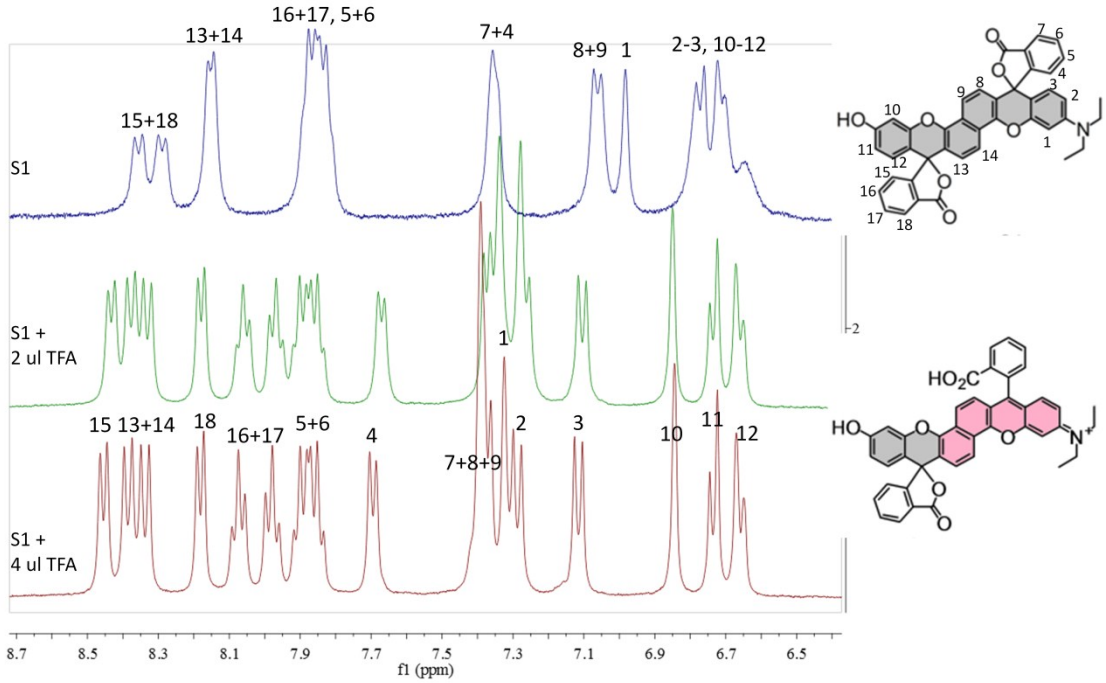

Fig. S8. The ^{1}H NMR (400 MHz) titration of **S1** towards TFA (in 80% CD_3OD and 20% DMSO-d_6).

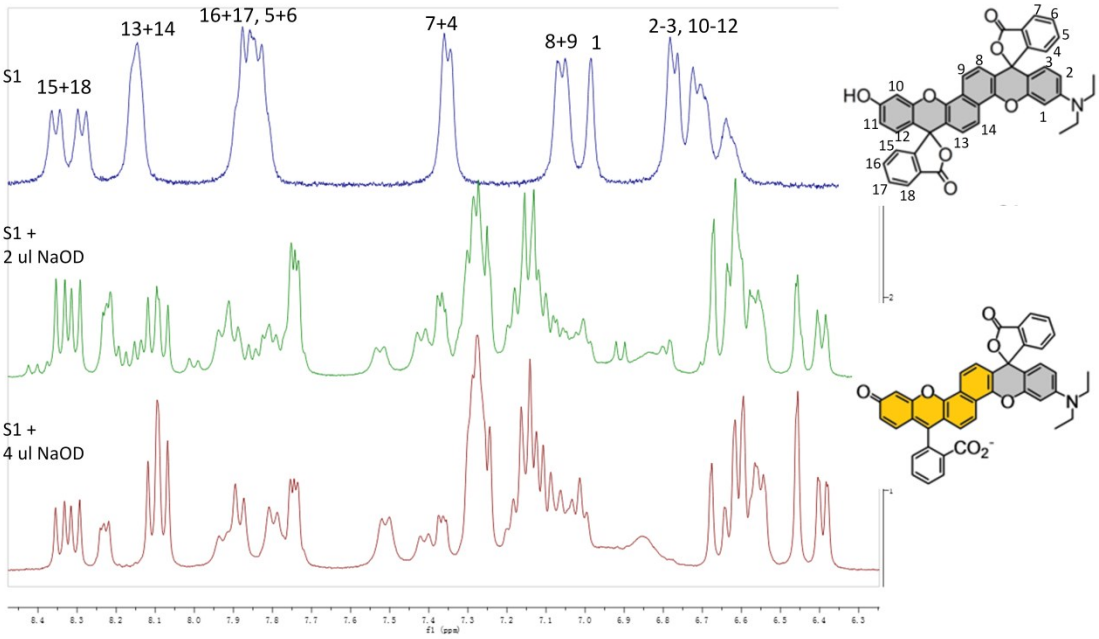

Fig. S9. The ^{1}H NMR (400 MHz) titration of **S1** towards NaOD (in 80% CD_3OD and 20% DMSO-d_6).

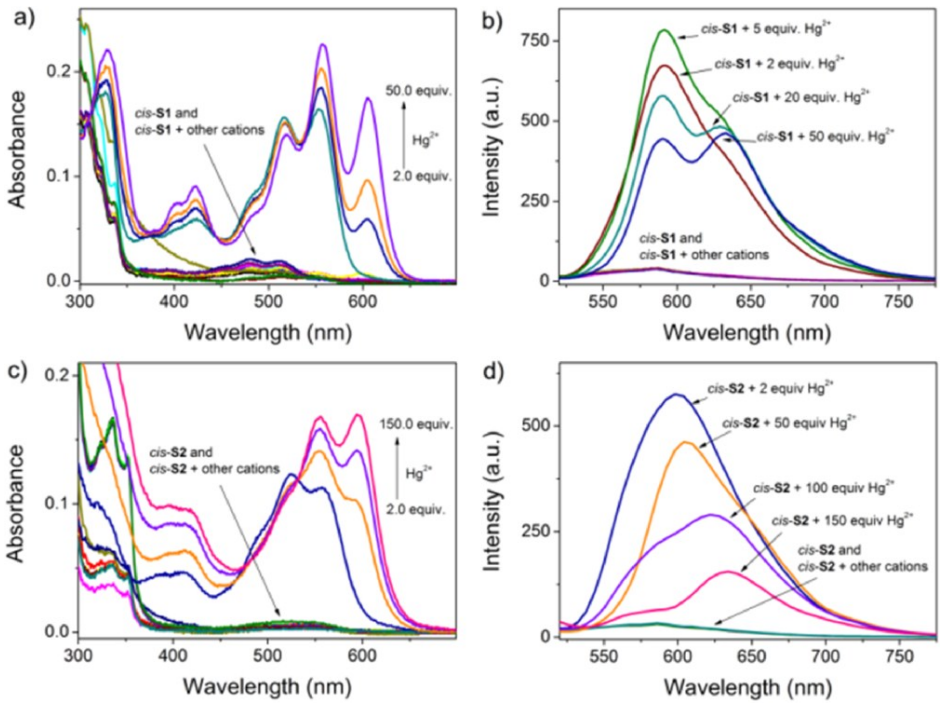

Fig. S10. UV-Vis absorption and fluorescence spectra of (a, b) *cis*-**S1** (5 μM) and (c, d) *cis*-**S2** (5 μM) in the presence of 10.0 equivalents (50 μM) of various metal ions and different concentrations of Hg^{2+} ions in methanol.

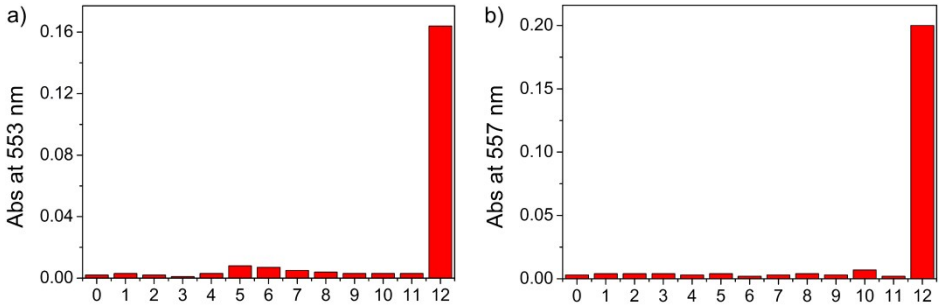

Fig. S11. The absorbance intensity of (a) **S1** (5 μM) and (b) **S2** (5 μM) in the presence of 10.0 equivalents of metal ions in methanol. 0: dye; 1: Na^{+}; 2: Ba^{2+}; 3: Ca^{2+}; 4: Cd^{2+}; 5: Co^{2+}; 6: Cu^{2+}; 7: Fe^{2+}; 8: Mg^{2+}; 9: Ni^{2+}; 10: Pb^{2+}; 11: Zn^{2+}; 12: Hg^{2+}.

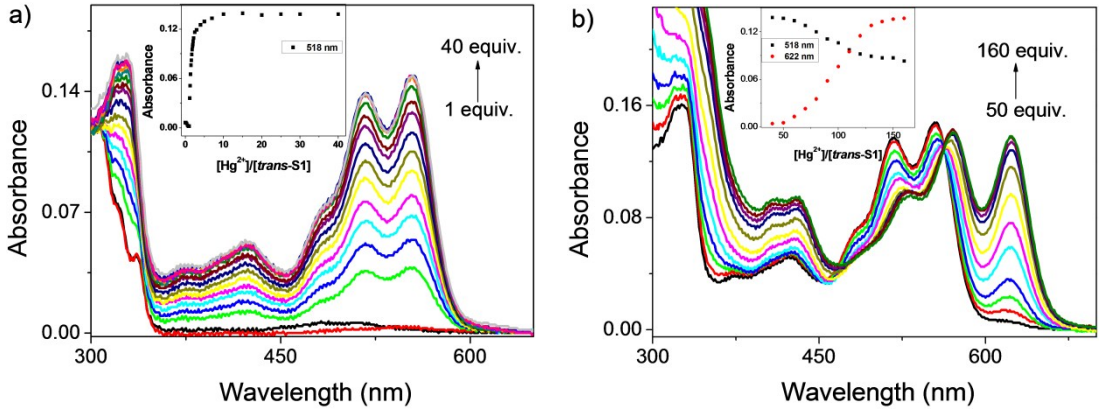

Fig. S12. a) UV-Vis absorption spectral changes of *trans*-**S1** (5 μM) in MeOH in the presence of a) low and b) high concentrations of Hg^{2+}; insets show the plot of absorbance intensity as a function of the concentration of Hg^{2+}.

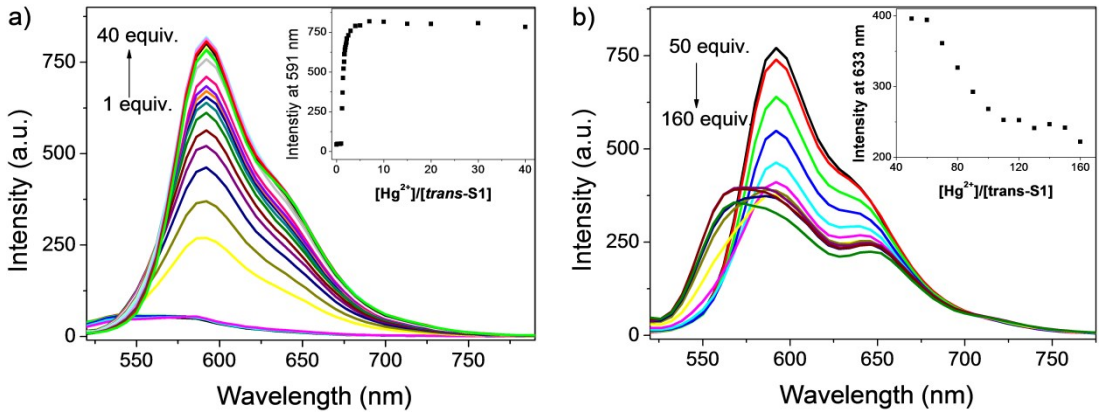

Fig. S13. a) Fluorescence spectral changes of *trans*-**S1** (5 μM) upon additions of a) low and b) high concentrations of Hg^{2+} in MeOH; insets show the plot of fluorescence emission intensity as a function of the concentration of Hg^{2+}.

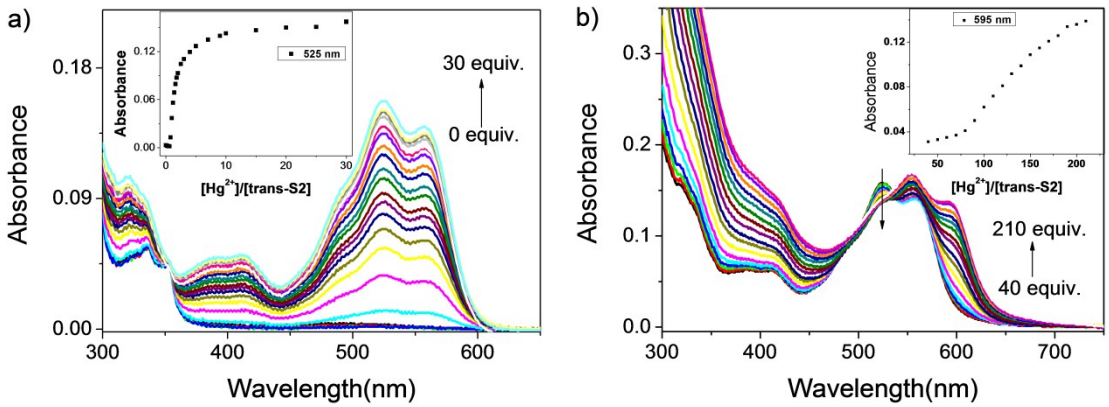

Fig. S14. a) UV-Vis absorption spectral changes of *trans*-**S2** (5 μM) in MeOH in the presence of a) low and b) high concentrations of Hg^{2+}; insets show the plot of absorbance intensity as a function of the concentration of Hg^{2+}.

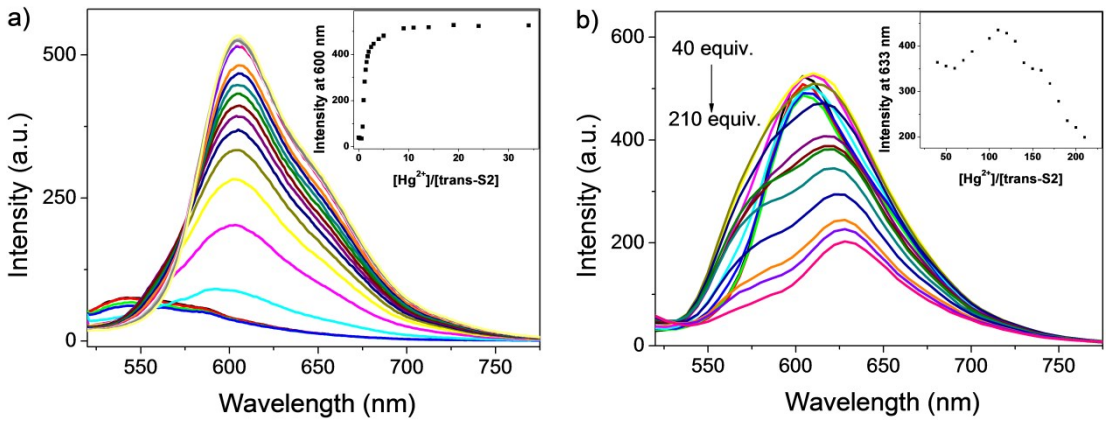

Fig. S15. a) Fluorescence spectral changes of *trans*-**S2** (5 μM) upon additions of a) low and b) high concentrations of Hg^{2+} in MeOH; insets show the plot of fluorescence emission intensity as a function of the concentration of Hg^{2+}.

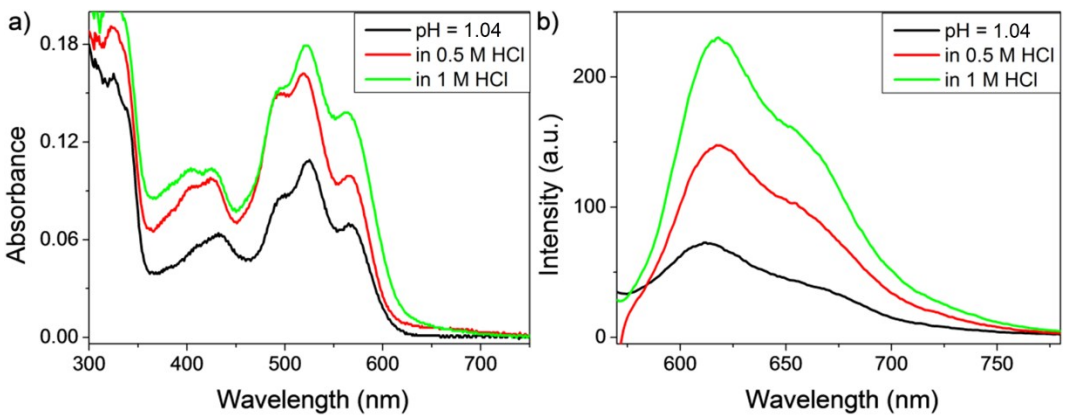

Fig. S16. a) Absorption and b) fluorescence spectra of **S1** (10 μM) in water with pH value of 1.04 and in the presence of different conditions of HCl concentration.

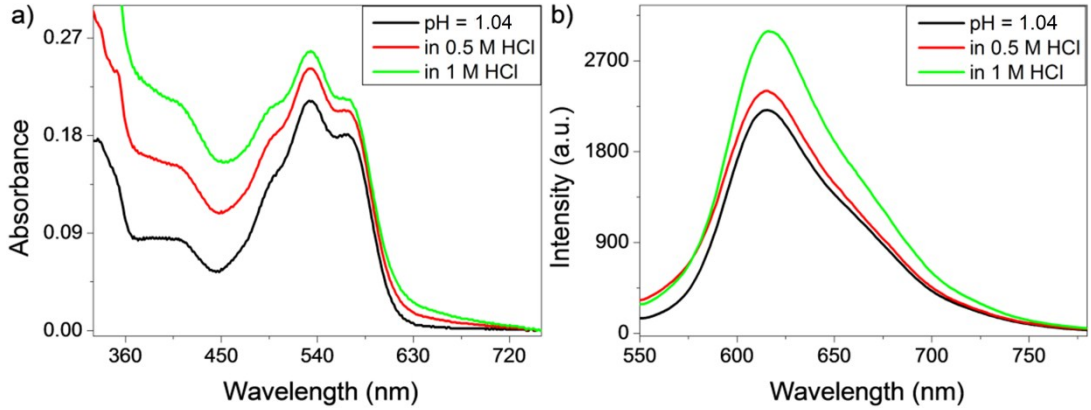

Fig. S17. a) Absorption and b) fluorescence spectra of **S2** (10 μM) in water with pH value of 1.04 and in the presence of different conditions of HCl concentration.

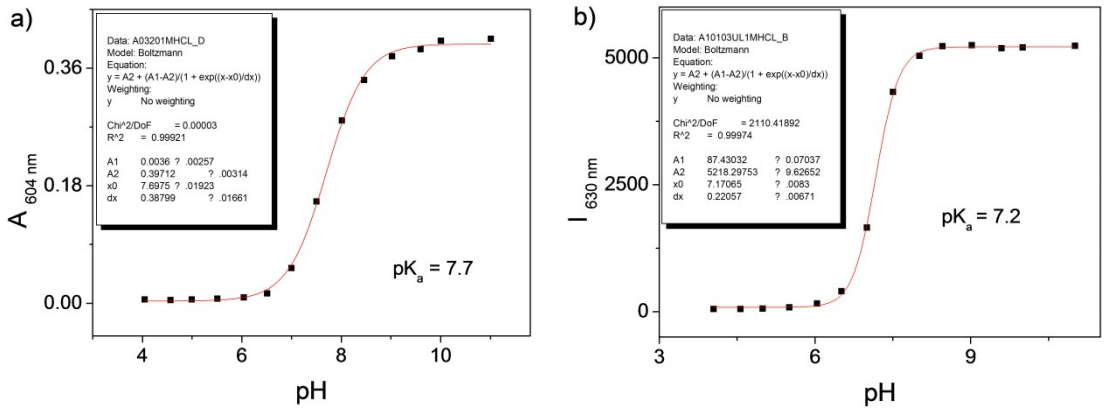

Fig. S18. a) The intensity of absorbance of **S1** at 604 nm in PBS (10 mM) at different pH; b) the intensity of fluorescence emission of **S1** at 630 nm in PBS (10 mM) at different pH.

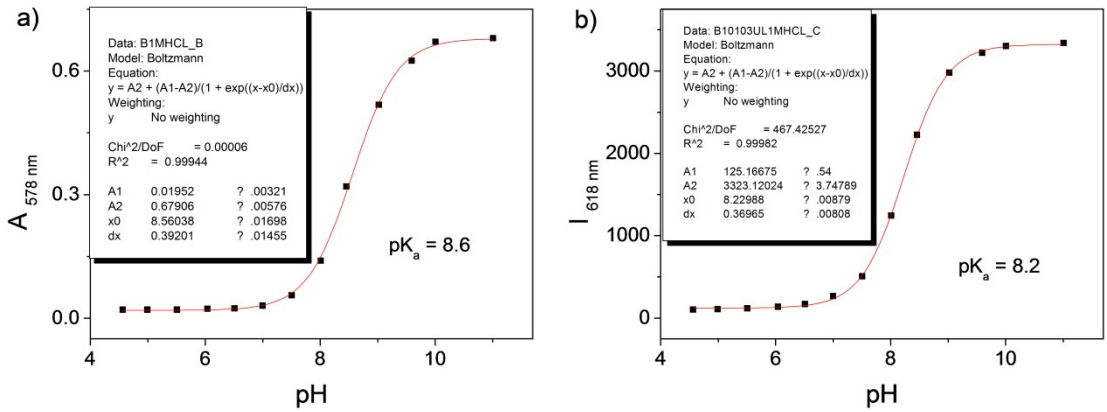

Fig. S19. a) The intensity of absorbance of **S2** (10 μM) at 578 nm in PBS (10 mM) at different pH; b) the intensity of fluorescence emission of **S2** (10 μM) at 618 nm in PBS (10 mM) at different pH.

a)

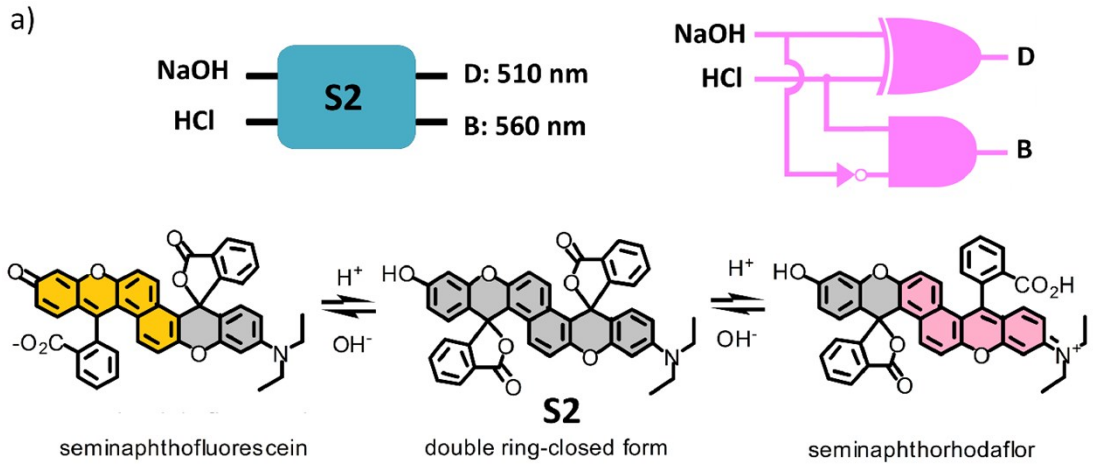

b)

Input		Output	
NaOH	HCl	XOR: D	INH: B
*I*1	*I*2	510 nm: *O*1	560 nm: *O*2
0	0	0 (low, 0.022)	0 (low, 0.004)
0	1	1 (high, 0.48)	1 (high, 0.52)
1	0	1 (high, 0.189)	0 (low, 0.008)
1	1	0 (low, 0.019)	0 (low, 0.003)

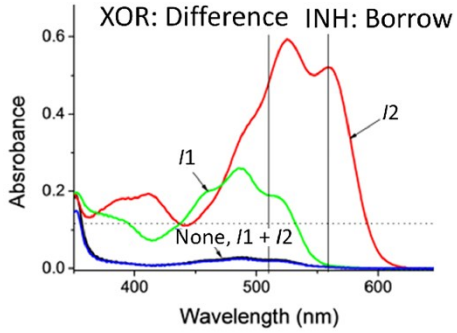

Fig. S20. (a) Schematic presentation of a half-subtractor (top right) and its molecular analogue (top left) and equilibration of **S2** among the double-ring-closed form and the mono-ring-opened seminaphthofluorescein and seminaphthorhodaflor forms (bottom). (b) Introduction of base (NaOH, *I*1)and acid (HCl, *I*2) inputs to a methanol solution of **S2** (20 μM) in its double-ring-closed form (**S2**) results in absorption changes (right) corresponding to the equivalent truth table of a half-subtractor logic circuit (left). Difference (D) and borrow (B) are recorded at 510 nm (*O*1) and 560 nm (*O*2), respectively. Outputs (*O*): 1 ($A > 0.12$), 0 ($A < 0.12$).

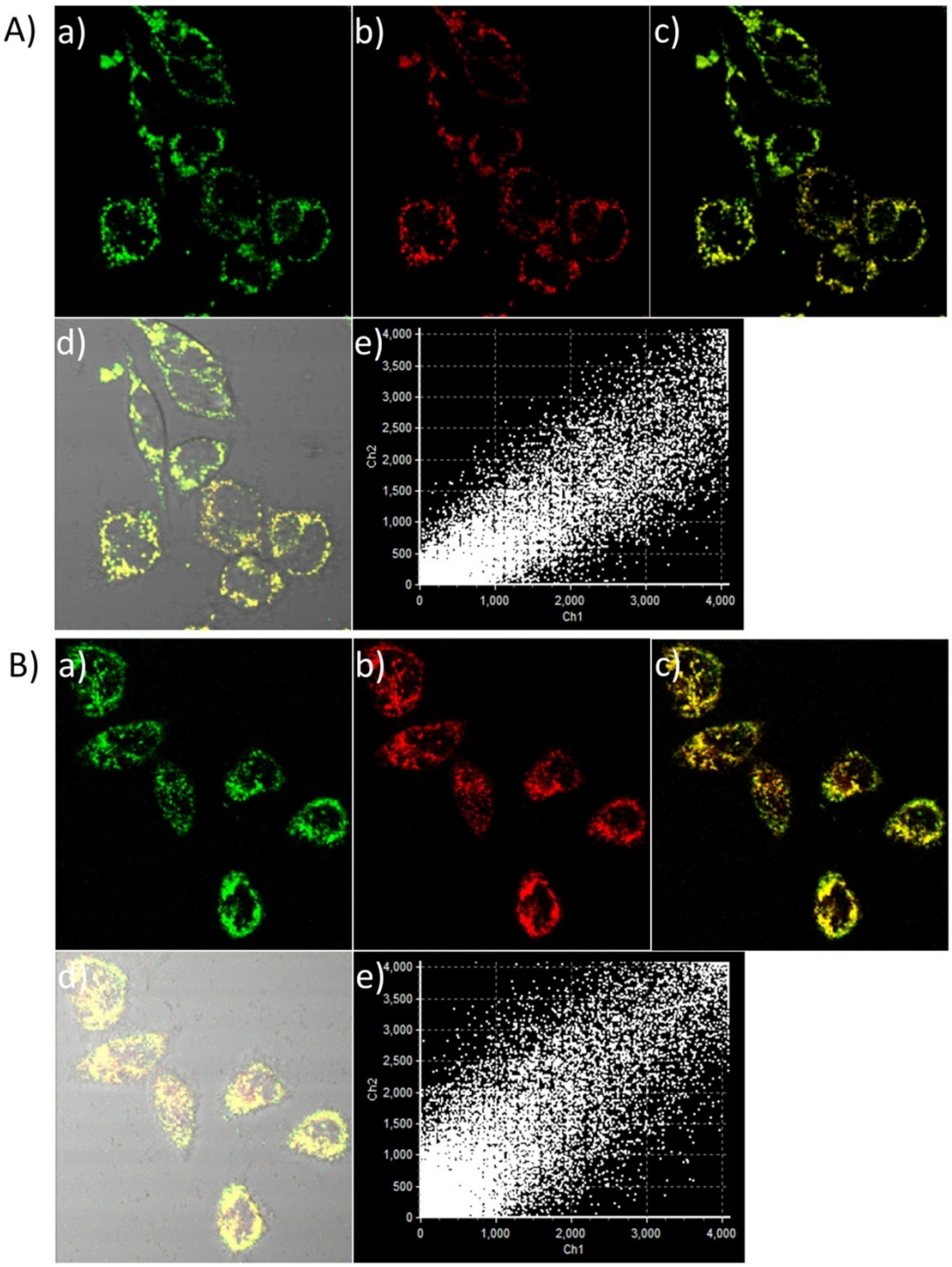

Fig. S21. Localization of *cis*-**S1** (A), *cis*-**S2** (B) in mitochondria in HeLa cells. Mito tracker Green (200 nM), *cis*-**S1** (5 μM), and *cis*-**S2** (5 μM) were loaded into HeLa cells for 30 min, respectively. a) Fluorescence image of MitoTracker Green. b) Fluorescence image of *cis*-**S1**, *cis*-**S2**, respectively. c) Merged images of *cis*-**S1** and *cis*-**S2** with MitoTracker Green, respectively. d) Merged images of bright field , *cis*-**S1,** or *cis*-**S2** and MitoTracker Green, respectively. e) Intensity correlation plot of LysoTracker and Mito tracker Green with dyes *cis*-**S1** or *cis*-**S2**, respectively.

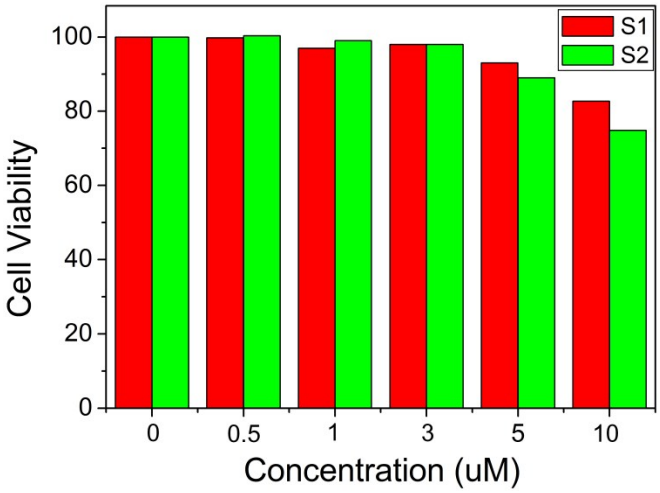

Fig. S22. Cytotoxicity of dyes **S1** and **S2** in HeLa cells. Cell viability values (%) estimated by MTT assays using L929 cells, cultured in the presence of 0-10 μM of dyes **S1** and **S2** for 24 h at 37 °C, respectively.

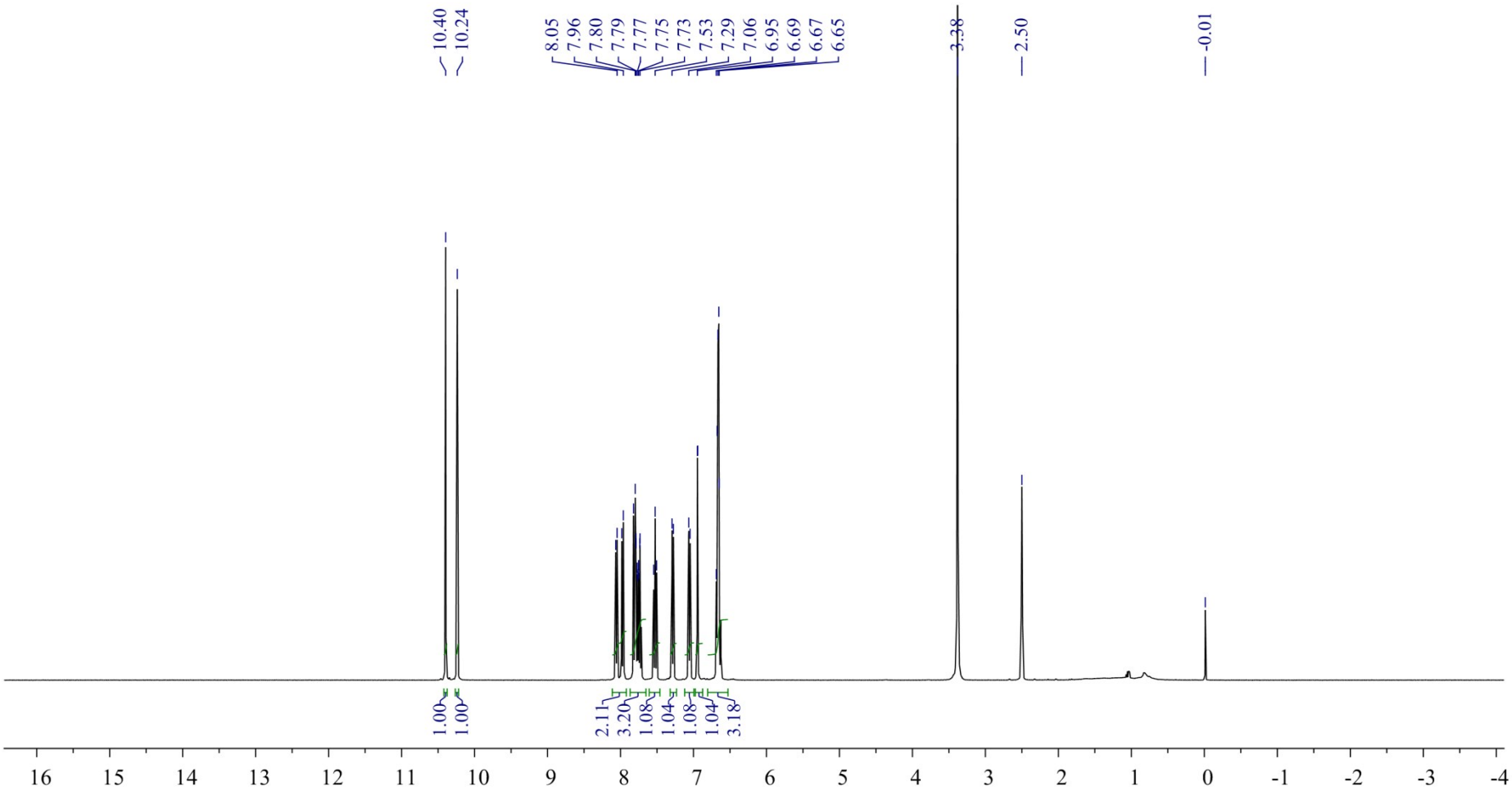

Fig. S23. ^{1}H NMR spectrum of **1** (400 MHz, DMSO-d_6).

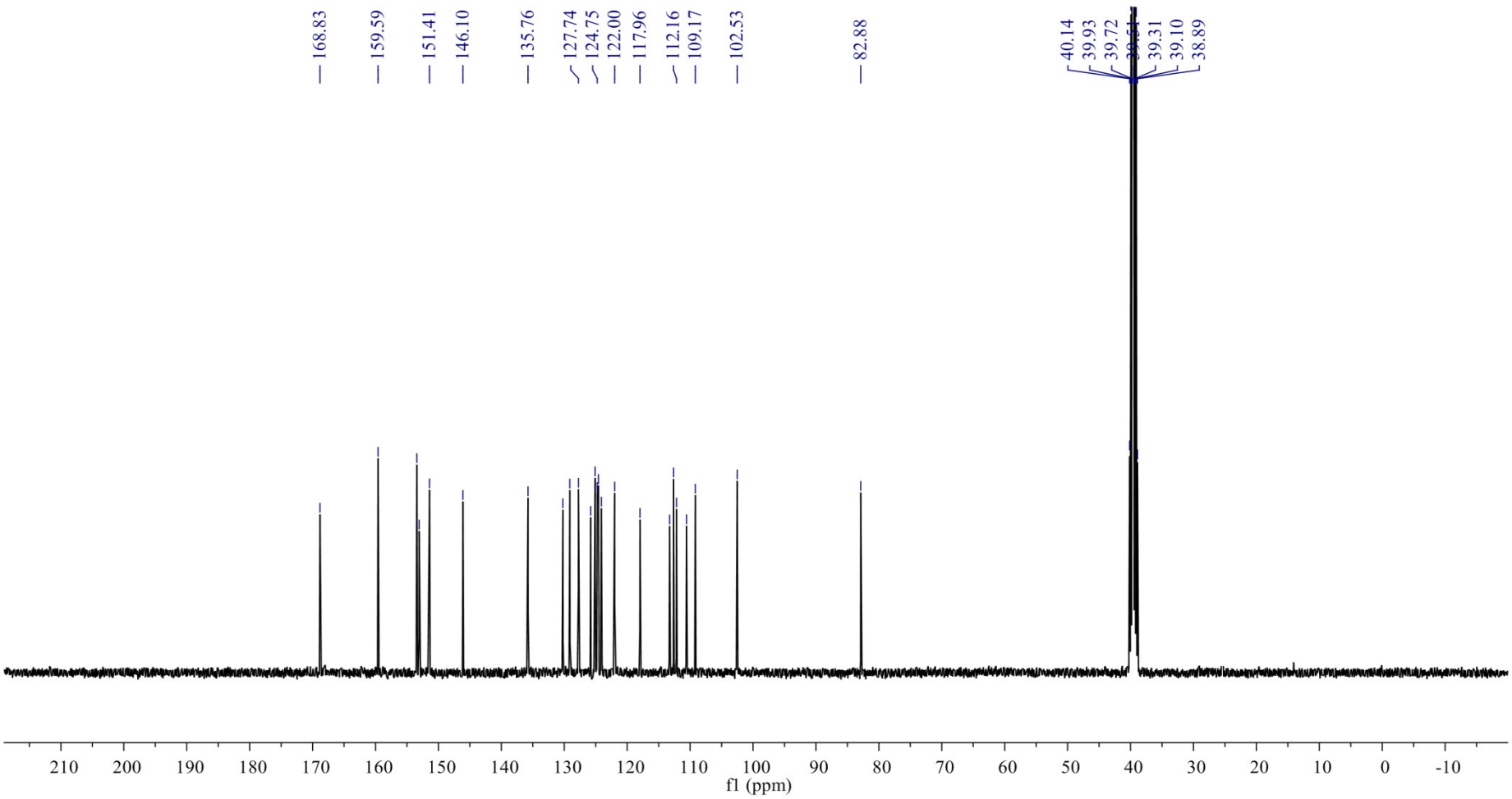

Fig. S24. ^{13}C NMR spectrum of **1** (100 MHz, DMSO-d_6).

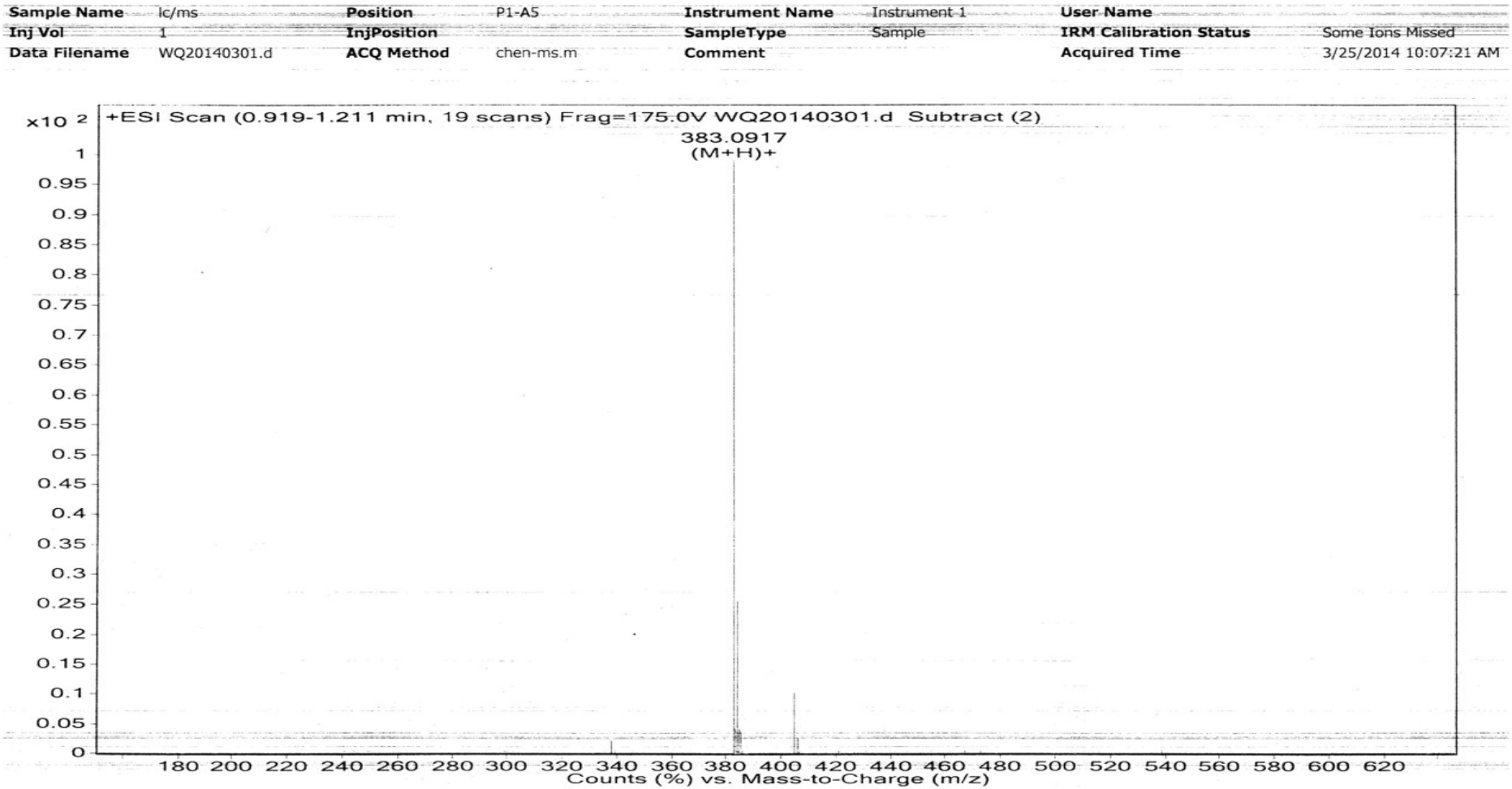

Fig. S25. HRMS of **1.** HRMS (ESI−TOF) *m*/*z* calcd for $C_{24}H_{15}O_5$ (M + H^+): 383.0920; found: 383.0917.

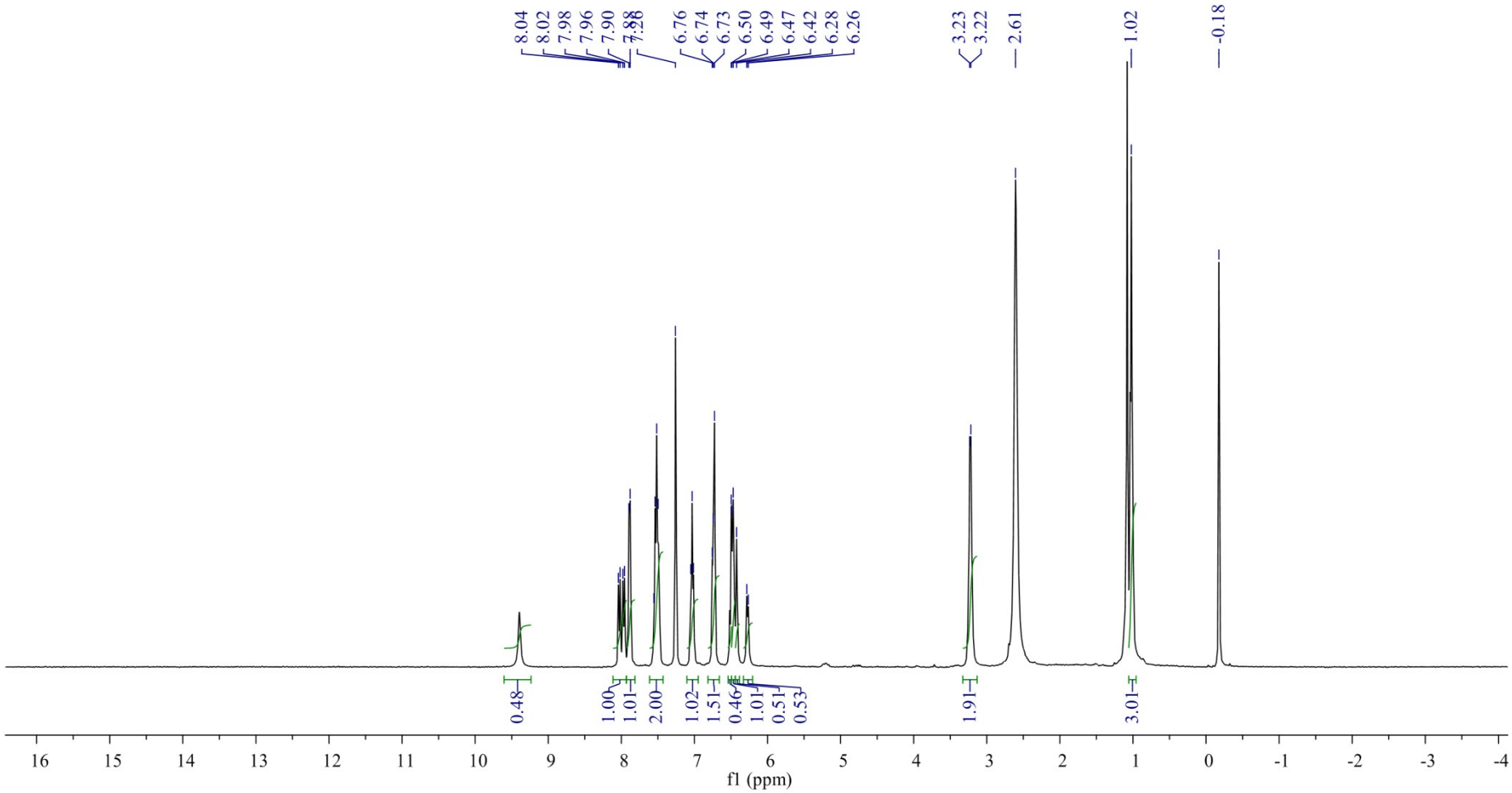

Fig. S26. ^{1}H NMR spectrum of *trans*-**S1** (400 MHz, $CDCl_3$ and DMSO-d_6).

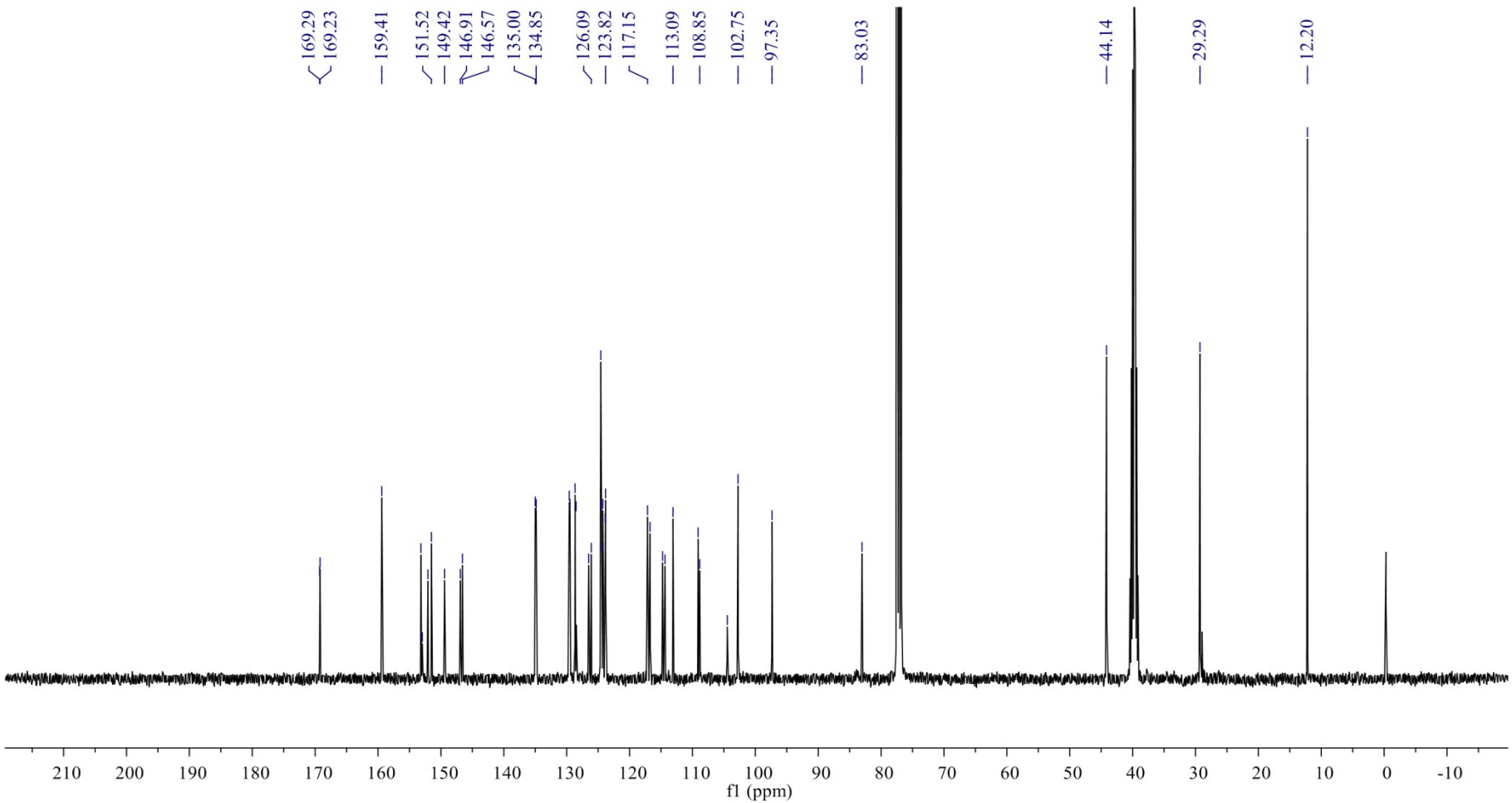

Fig. S27. ^{13}C NMR spectrum of *trans*-**S1** (100 MHz, $CDCl_3$ and DMSO-d_6).

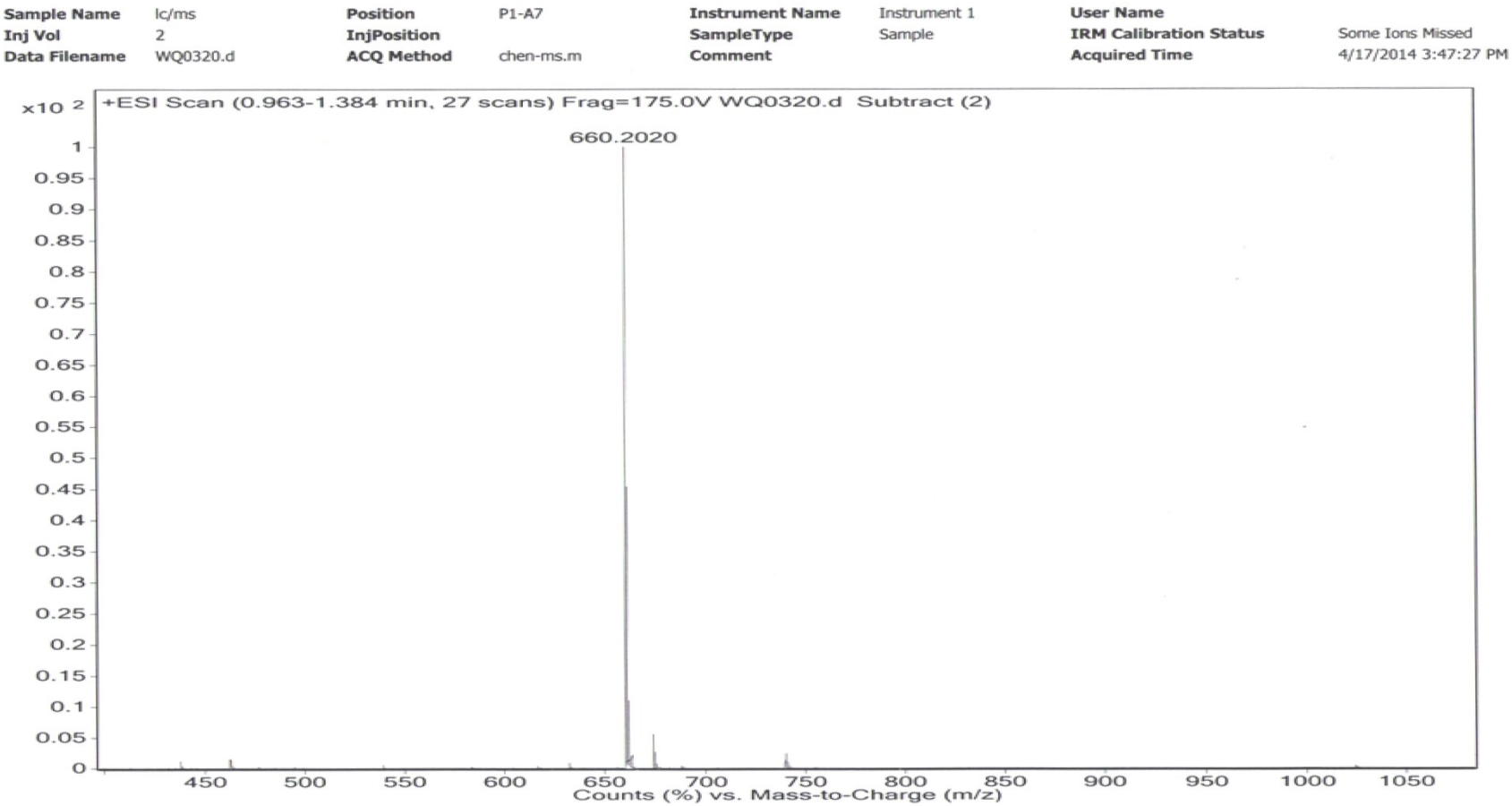

Fig. S28. HRMS of *trans*-**S1.** HRMS (ESI−TOF) *m*/*z* calcd for $C_{42}H_{30}NO_7$ (M + H^+): 660.2022; found: 660.2020.

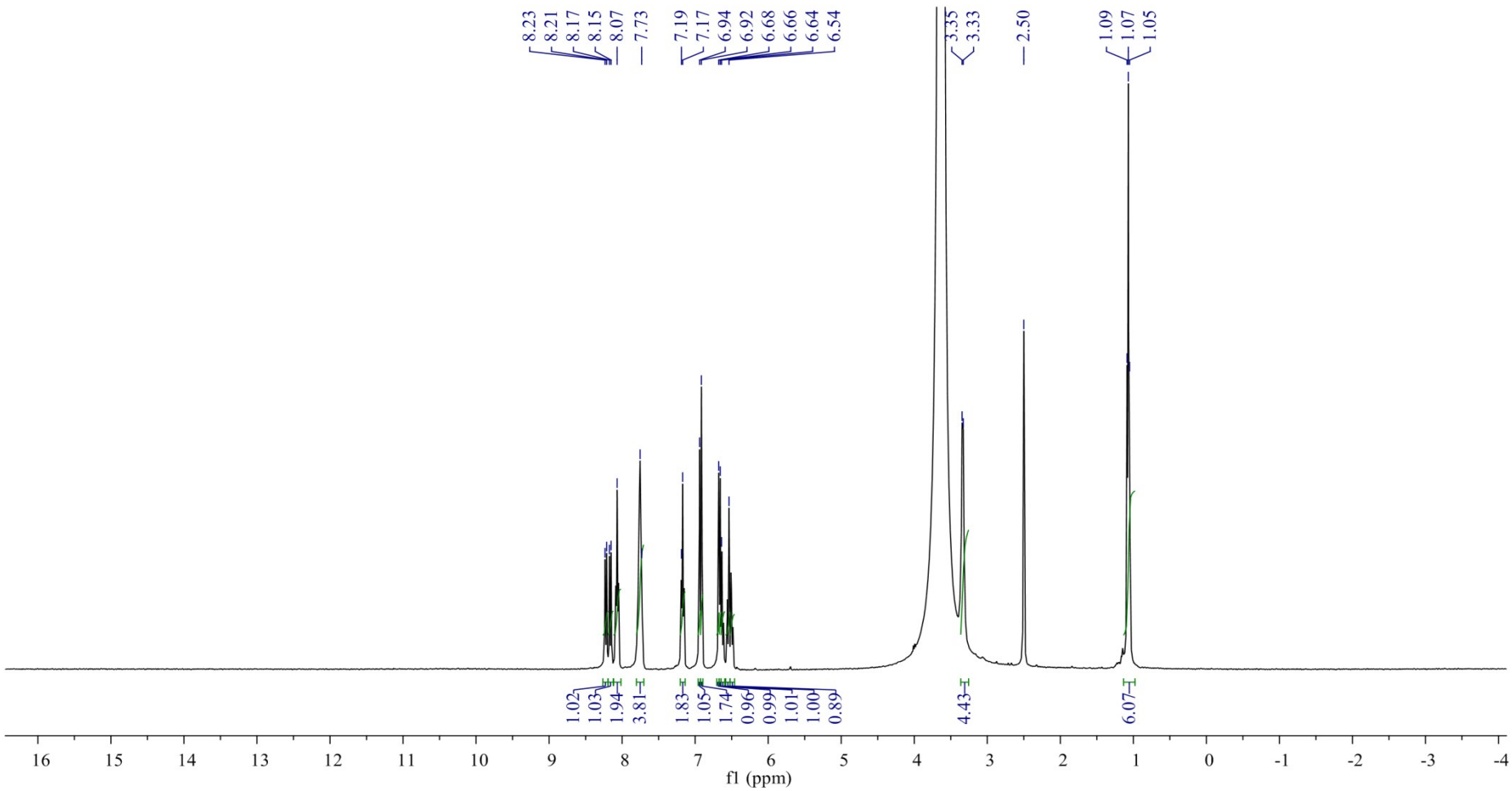

Fig. S29. ^{1}H NMR spectrum of *cis*-**S1** (400 MHz, DMSO-d_6).

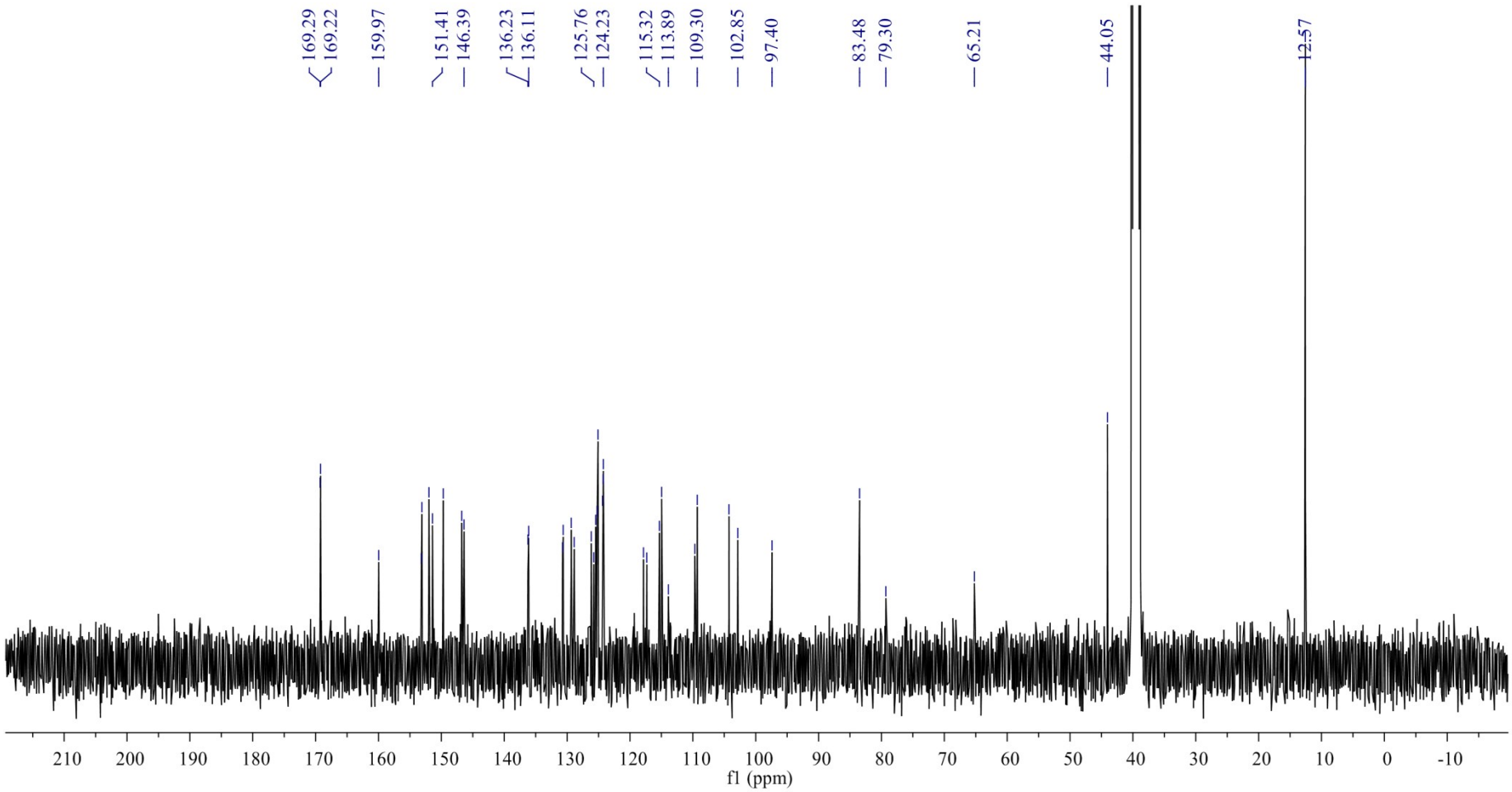

Fig. S30. ^{13}C NMR spectrum of *cis*-**S1** (100 MHz, DMSO-d_6).

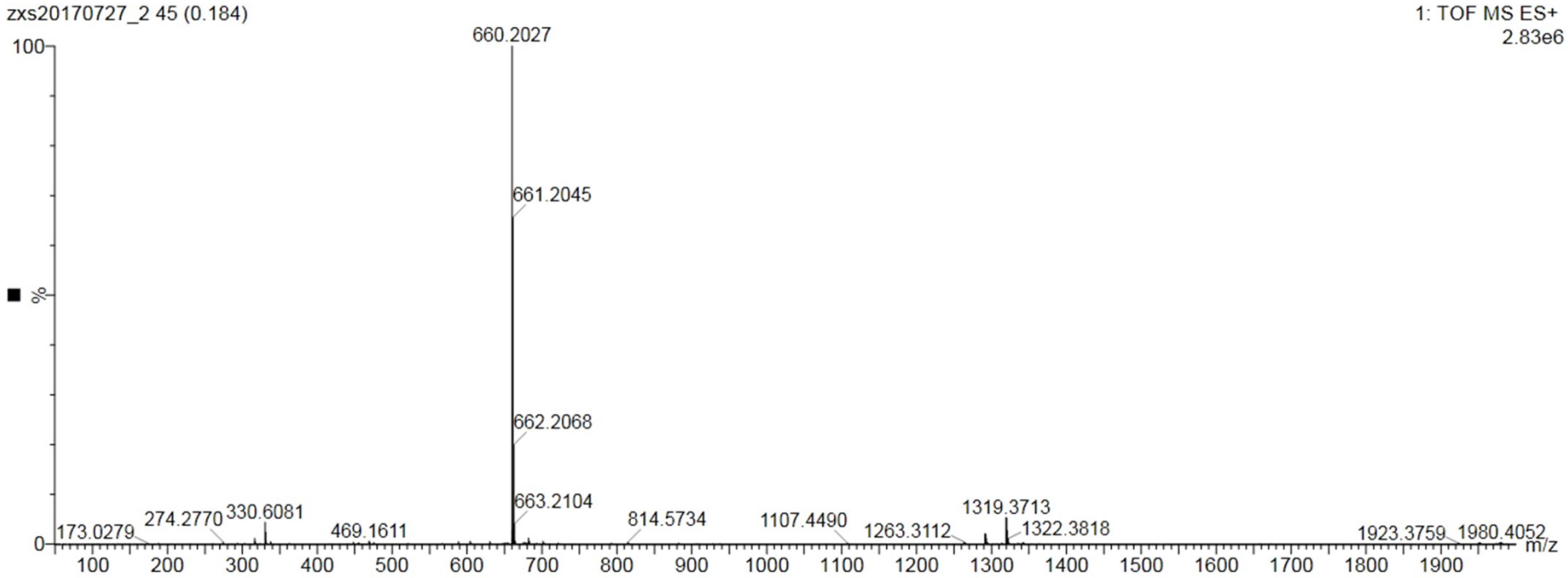

Fig. S31. HRMS of *cis*-**S1**. HRMS (ESI−TOF) *m*/*z* calcd for $C_{42}H_{30}NO_7$ (M + H^+): 660.2022; found: 660.2027.

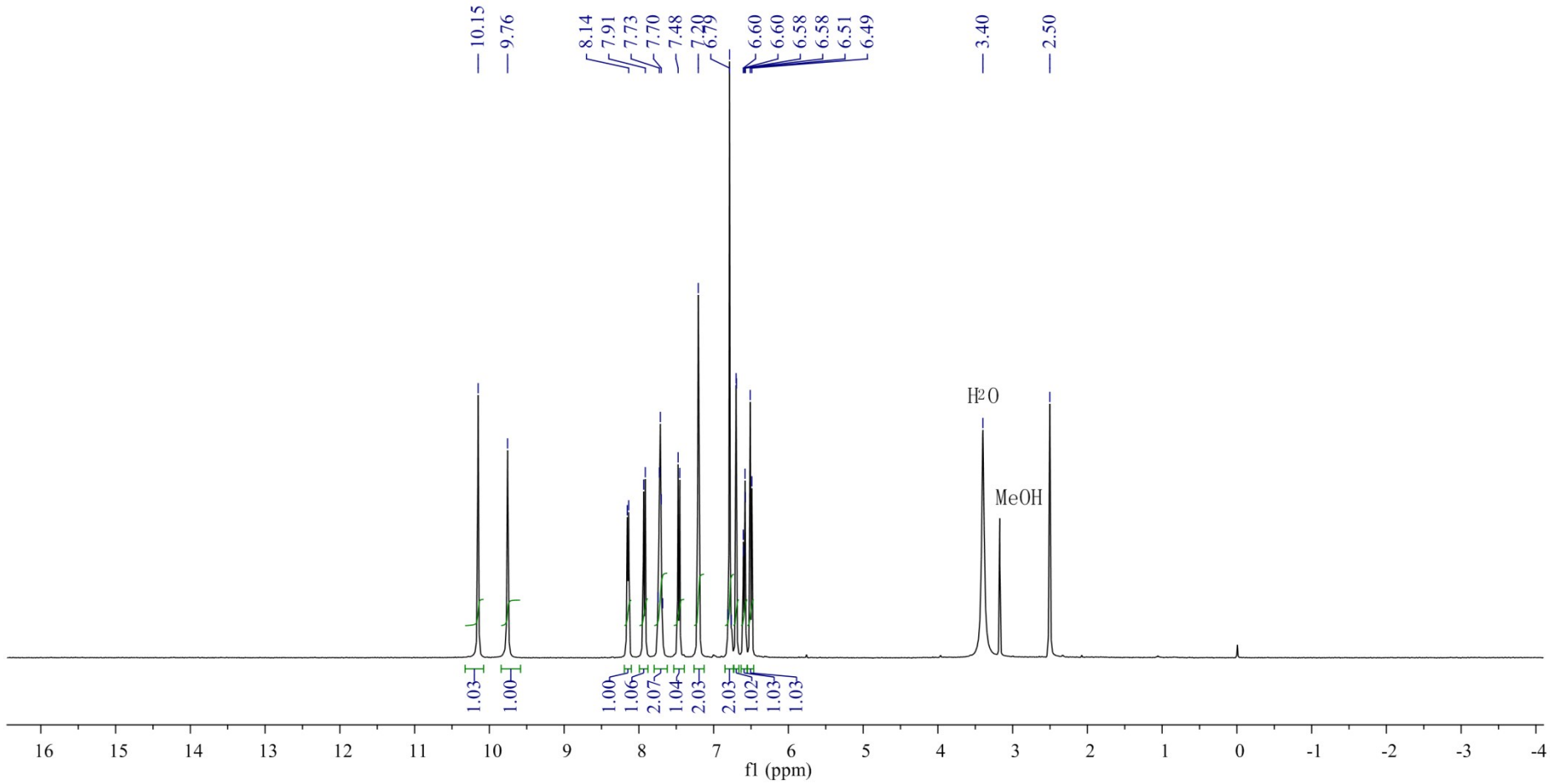

Fig. S32. ^{1}H NMR spectrum of **2** (400 MHz, DMSO-d_6).

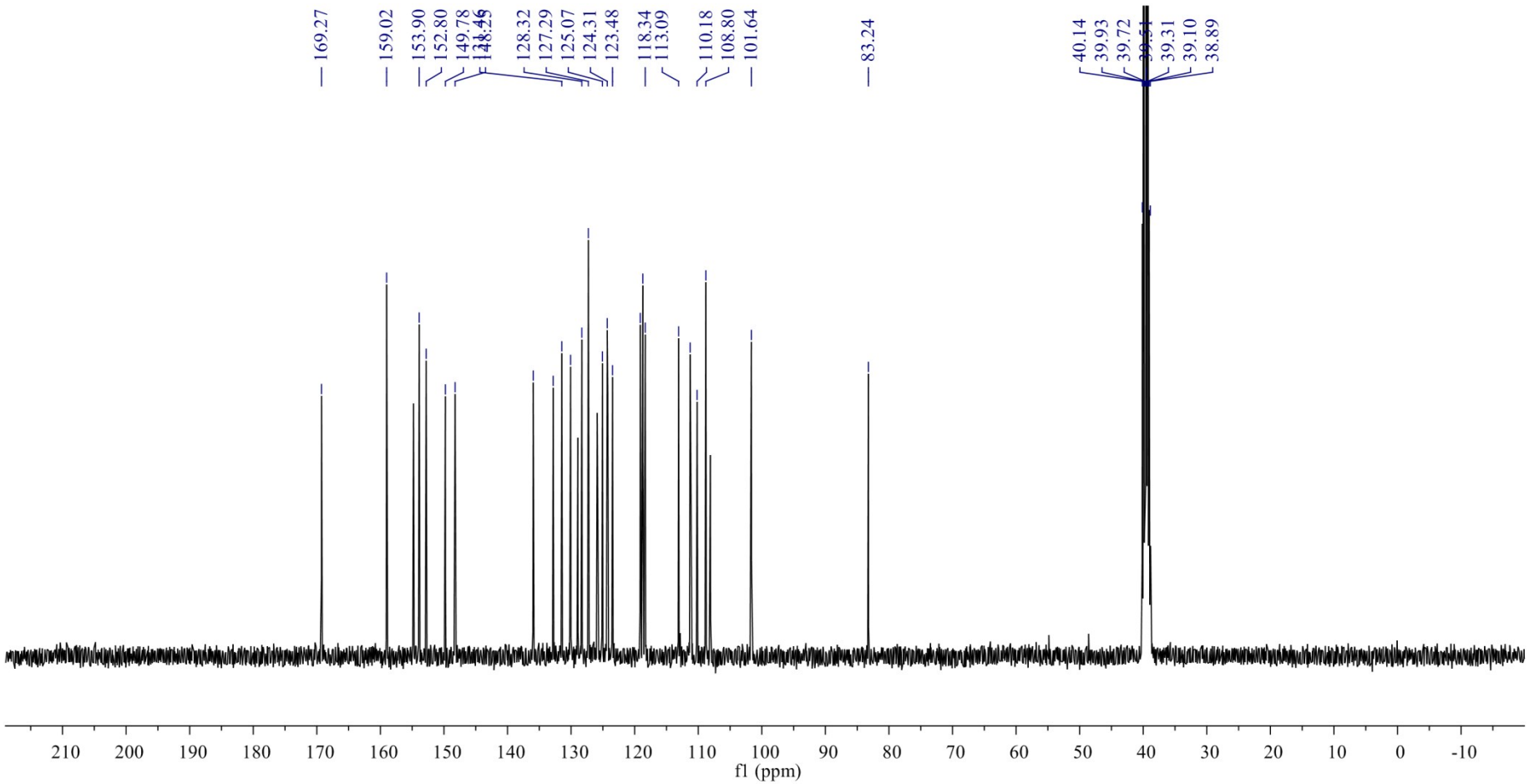

Fig. S33. ^{13}C NMR spectrum of **2** (100 MHz, DMSO-d_6).

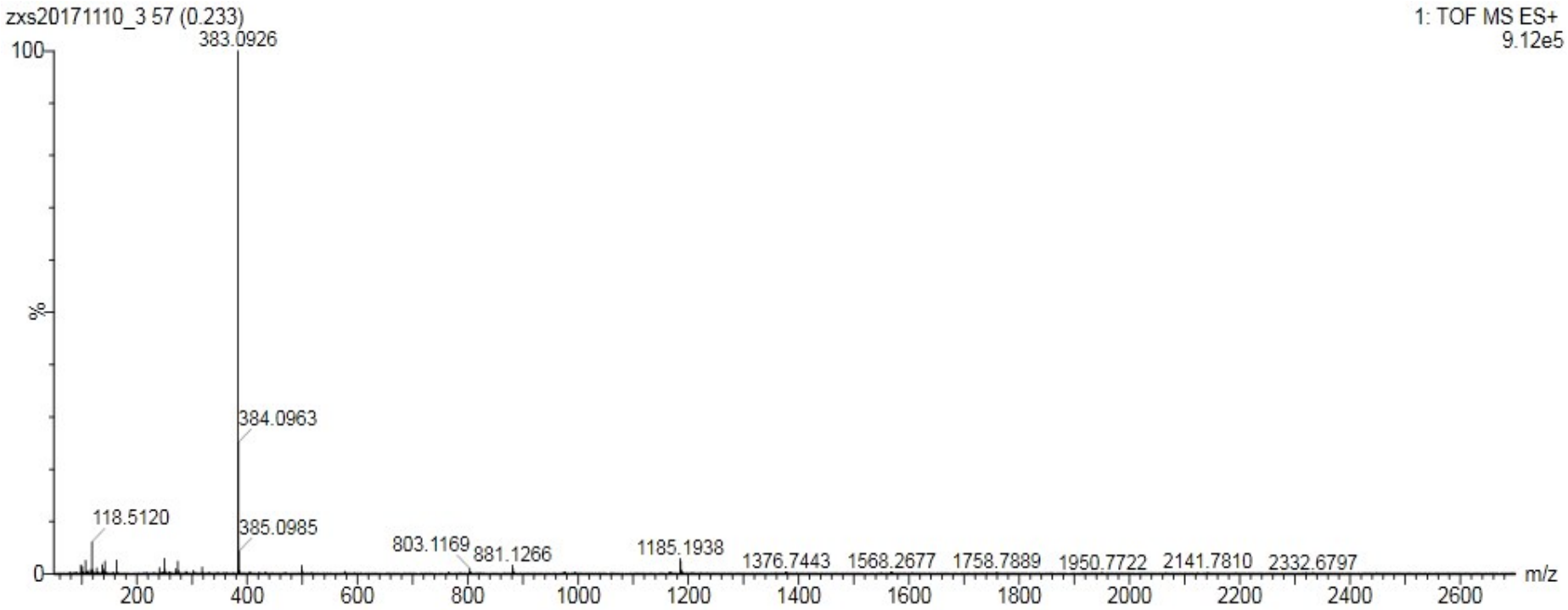

Fig. S34. HRMS of **2.** HRMS (ESI−TOF) *m/z* calcd for $C_{24}H_{15}O_5$ (M + H^+): 383.0919; found: 383.0926.

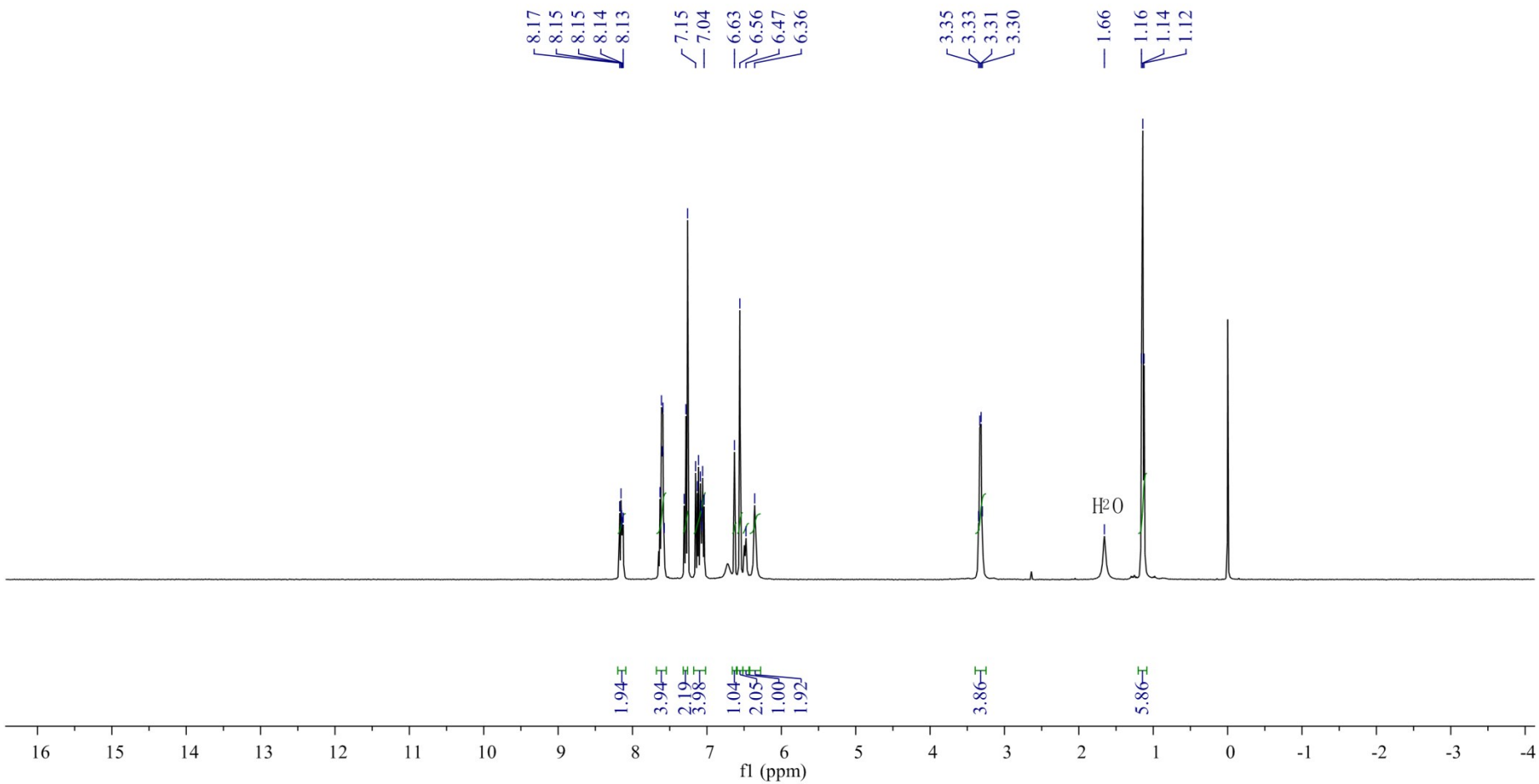

Fig. S35. ^{1}H NMR spectrum of *trans*-**S*2*** (400 MHz, $CDCl_3$, with 1% TFA).

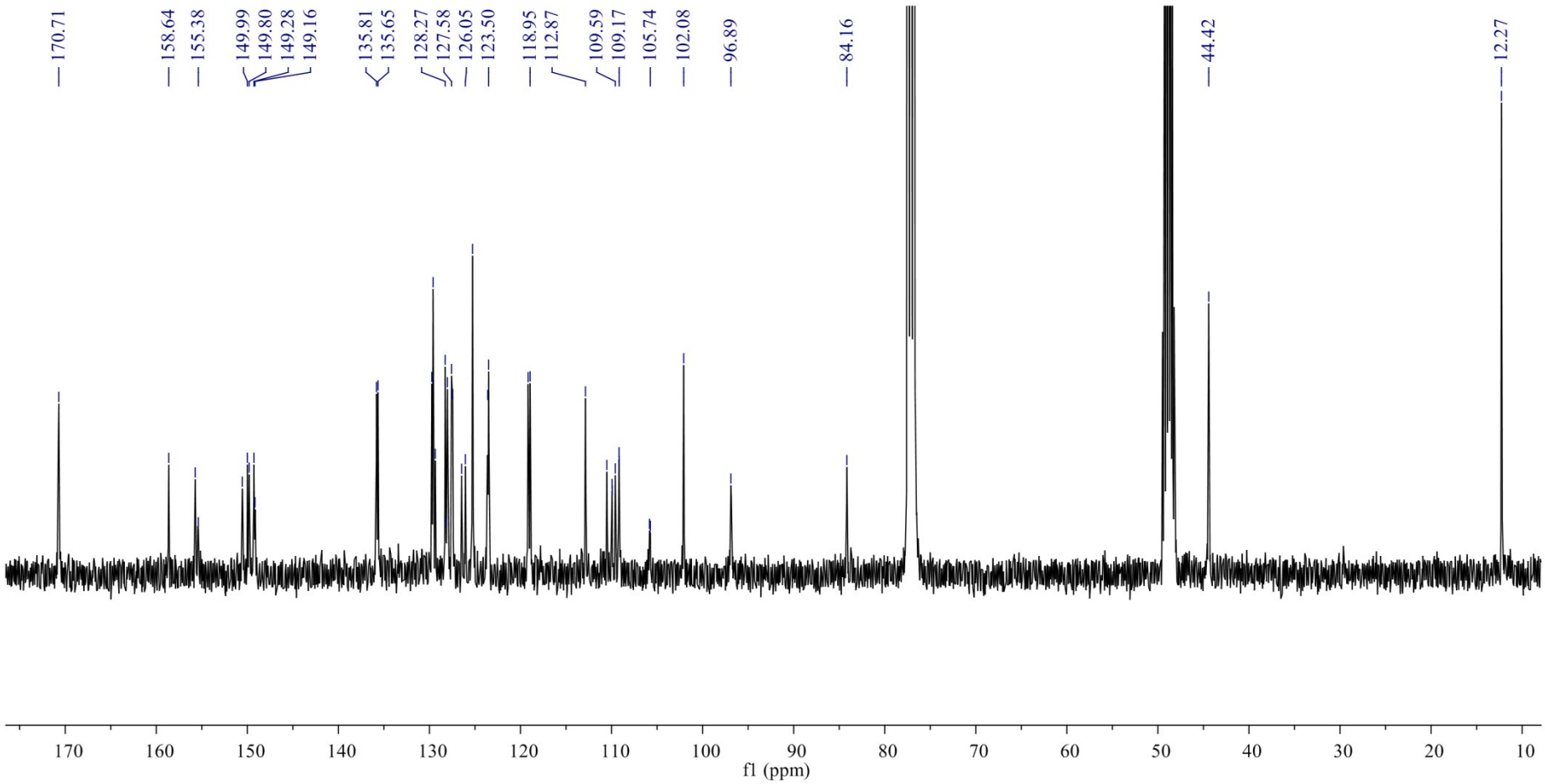

Fig. S36. ^{13}C NMR spectrum of *trans*-**S2** (100 MHz, CDCl3 and CD_3OD).

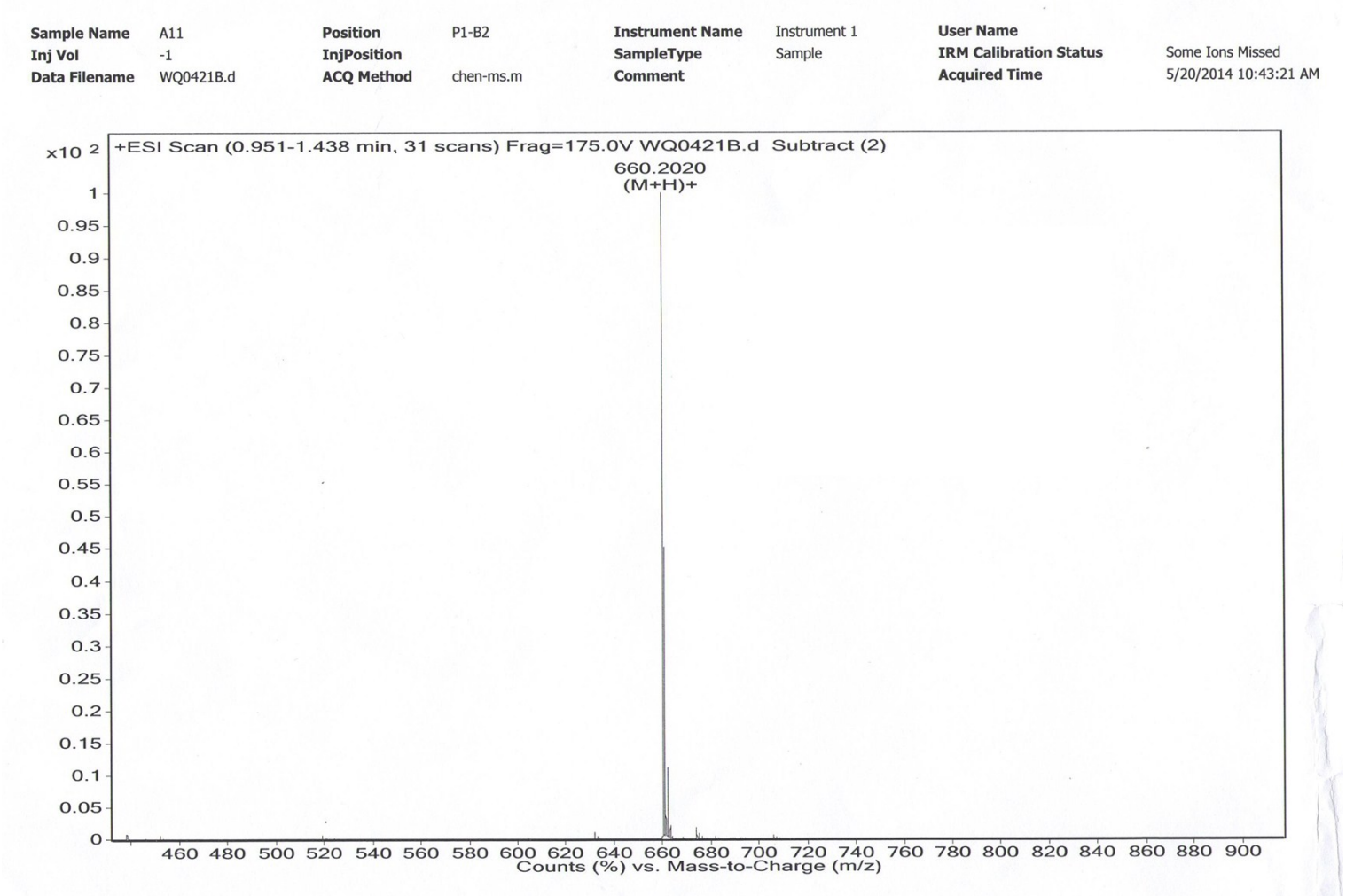

Fig. S37. HRMS of *trans*-**S2.** HRMS (ESI−TOF) *m*/*z* calcd for $C_{42}H_{30}NO_7$ (M + H^+): 660.2022; found: 660.2020.

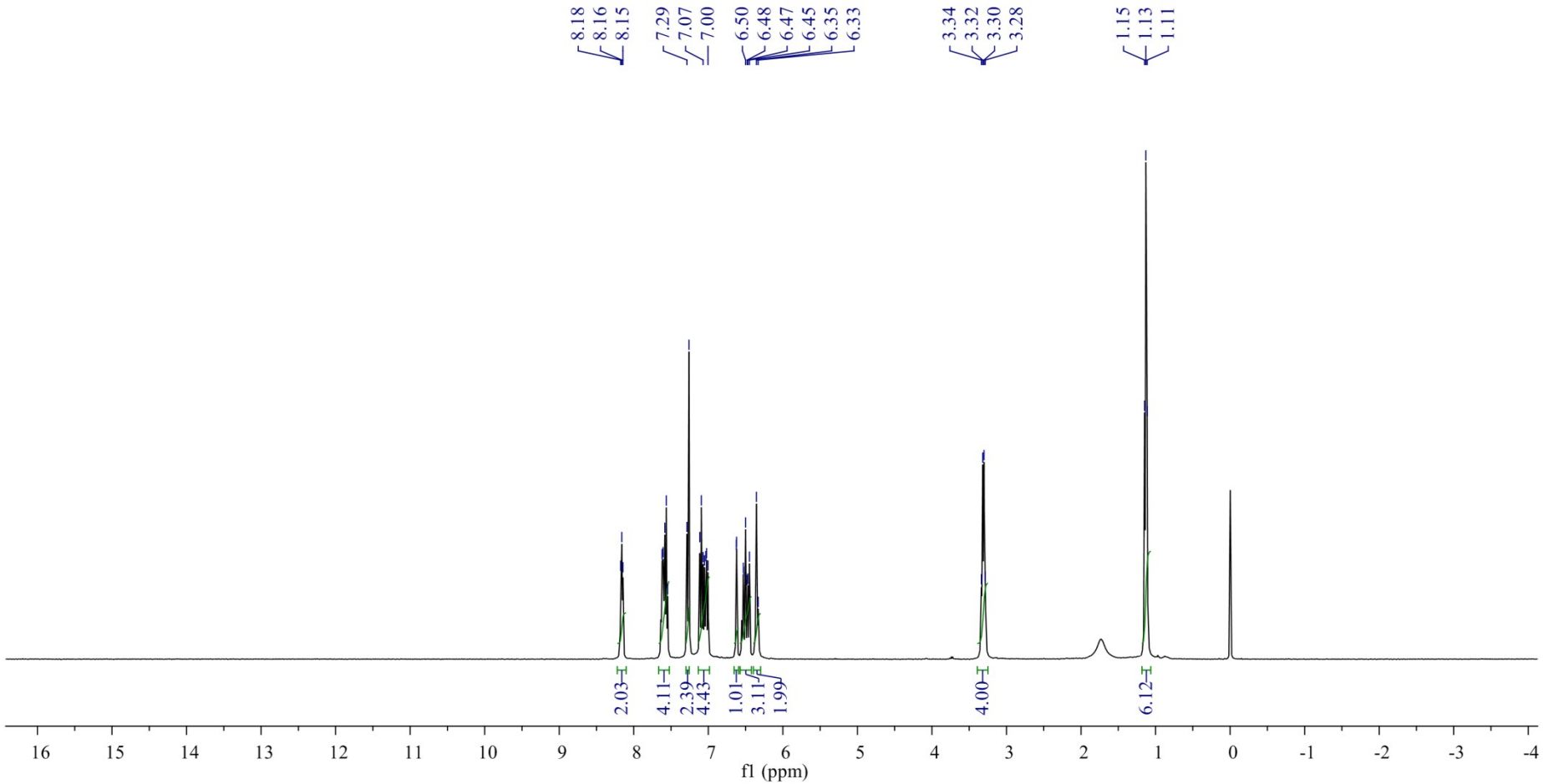

Fig. S38. ^{1}H NMR spectrum of *cis*-**S*2*** (400 MHz, $CDCl_3$).

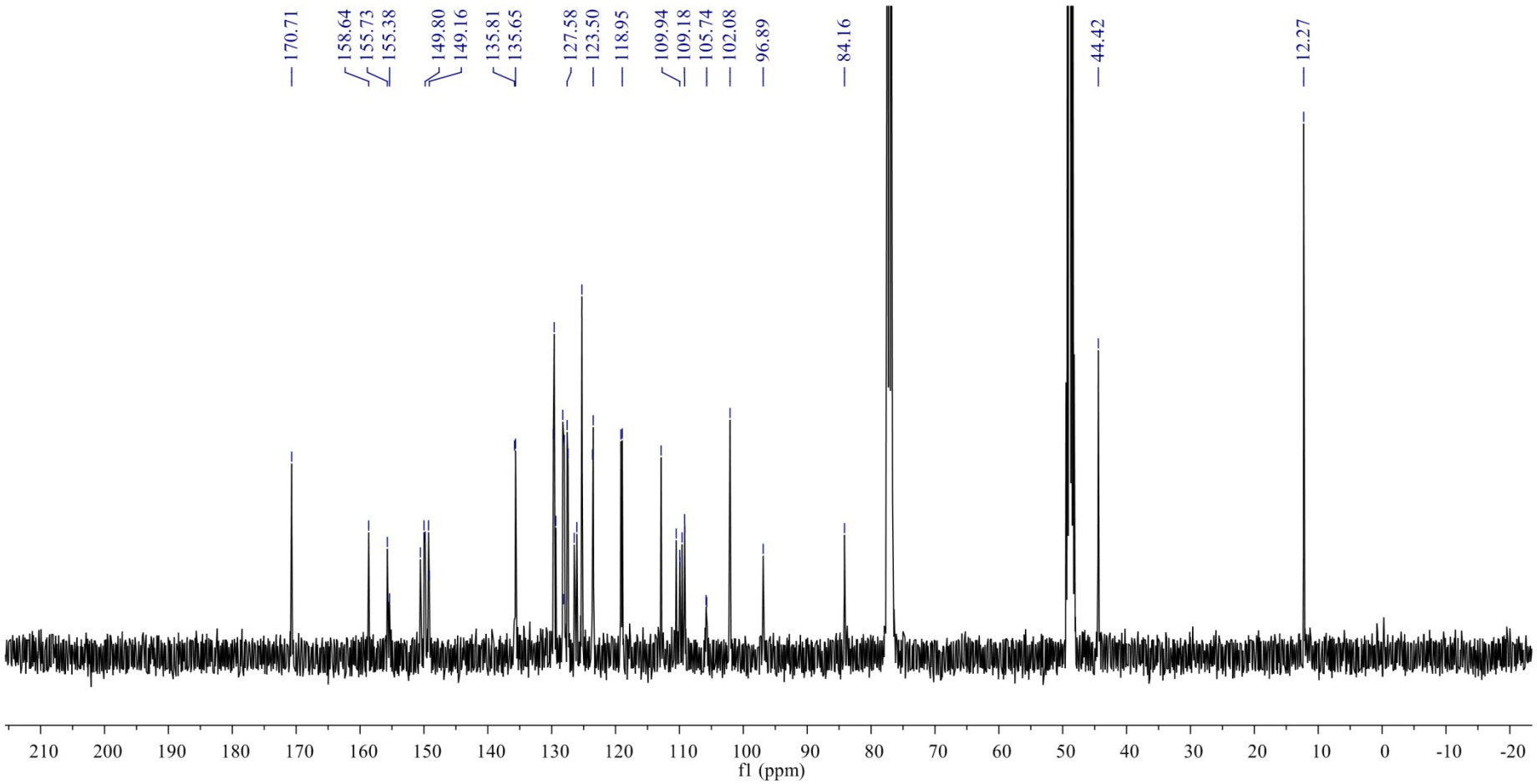

Fig. S39. ^{13}C NMR spectrum of *cis*-**S2** (100 MHz, CDCl3 and CD_3OD).

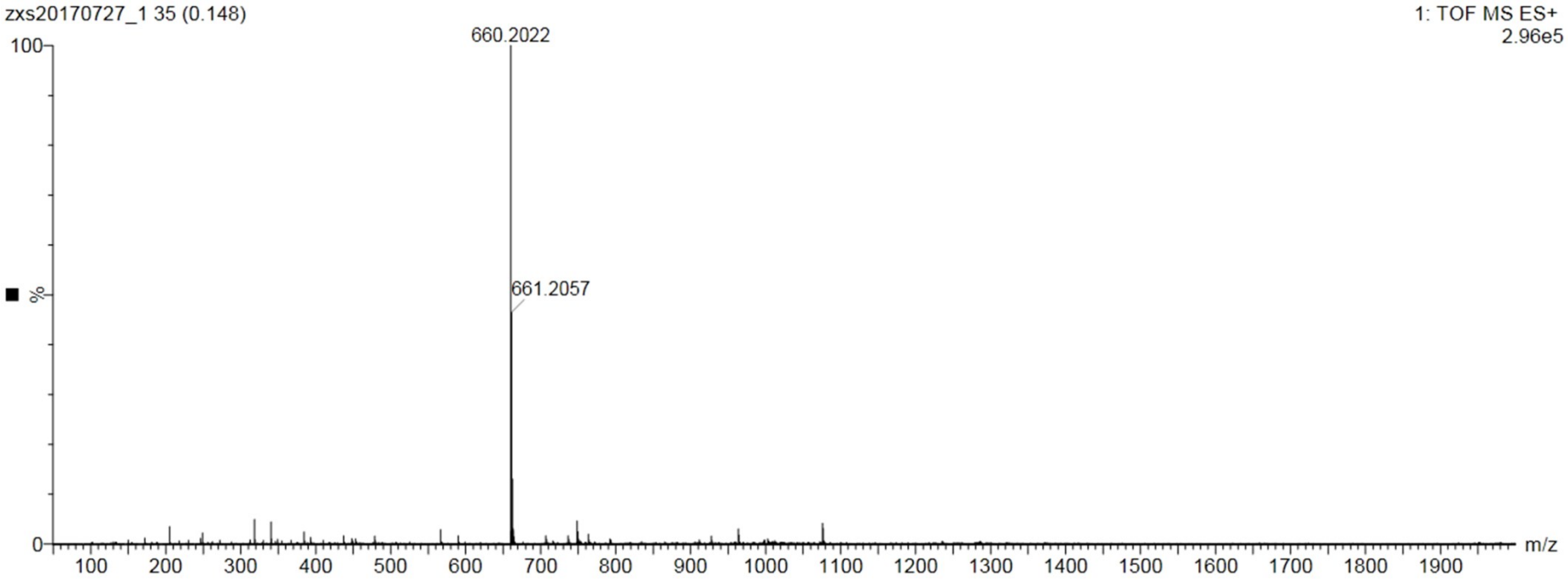

Fig. S40. HRMS of *cis*-**S2**. HRMS (ESI−TOF) *m*/*z* calcd for $C_{42}H_{30}NO_7$ (M + H^+): 660.2022; found: 660.2022.